

Article

Sensing Methodologies in Agriculture for Monitoring Biotic Stress in Plants Due to Pathogens and Pests

Bhuwan Kashyap *  and Ratnesh Kumar 

Department of Electrical and Computer Engineering, Iowa State University, Ames, IA 50010, USA; rkumar@iastate.edu

* Correspondence: bkashyap@iastate.edu

Abstract: Reducing agricultural losses is an effective way to sustainably increase agricultural output efficiency to meet our present and future needs for food, fiber, fodder, and fuel. Our ever-improving understanding of the ways in which plants respond to stress, biotic and abiotic, has led to the development of innovative sensing technologies for detecting crop stresses/stressors and deploying efficient measures. This article aims to present the current state of the methodologies applied in the field of agriculture towards the detection of biotic stress in crops. Key sensing methodologies for plant pathogen (or phytopathogen), as well as herbivorous insects/pests are presented, where the working principles are described, and key recent works discussed. The detection methods overviewed for phytopathogen-related stress identification include nucleic acid-based methods, immunological methods, imaging-based techniques, spectroscopic methods, phytohormone biosensing methods, monitoring methods for plant volatiles, and active remote sensing technologies. Whereas the pest-related sensing techniques include machine-vision-based methods, pest acoustic-emission sensors, and volatile organic compound-based stress monitoring methods. Additionally, Comparisons have been made between different sensing techniques as well as recently reported works, where the strengths and limitations are identified. Finally, the prospective future directions for monitoring biotic stress in crops are discussed.

Keywords: biosensors; hyperspectral; thermography; electrochemical; hormones; fluorescence; acoustic; spectroscopy; remote sensing; volatile organic compounds



Citation: Kashyap, B.; Kumar, R. Sensing Methodologies in Agriculture for Monitoring Biotic Stress in Plants Due to Pathogens and Pests. *Inventions* **2021**, *6*, 29. <https://doi.org/10.3390/inventions6020029>

Academic Editor: Konstantinos Arvanitis

Received: 1 March 2021

Accepted: 20 April 2021

Published: 22 April 2021

Publisher's Note: MDPI stays neutral with regard to jurisdictional claims in published maps and institutional affiliations.



Copyright: © 2021 by the authors. Licensee MDPI, Basel, Switzerland. This article is an open access article distributed under the terms and conditions of the Creative Commons Attribution (CC BY) license (<https://creativecommons.org/licenses/by/4.0/>).

1. Introduction

Global demand for food, water, and energy, with climate change and increasing variability in growing conditions, are among the key defining challenges of our time. According to the United Nations, the global population is expected to reach 9.55 billion by the year 2050 and 11.2 billion in 2100 [1], and the demand for food is expected to increase anywhere between 59% to 98% by 2050 [2]. Considering the unpredictability in climate, reduced land fertility from drought, erosion, and poor management, and agriculture's impact on the environment and the ever-increasing public expectation for implementing sustainable practices, achieving sustainability in agriculture has never been more important. In order to achieve the agricultural output goals in a sustainable fashion, we not only need to improve crop production efficiency through precision resource management but also reduce yield losses due to stresses in plants.

Presently, an estimated average of 21.5% of wheat, 30% of rice, 22.5% of maize, 17.2% of potato, and 21.4% of soybean yields are lost due to pests and diseases, globally [3]. Overall, an estimated 20% to 40% of all crop yield losses are caused by *pests and plant pathogens (phytopathogens)*, worldwide [4]. Losses of staple food crops such as, rice, wheat, maize, and potatoes directly impact food security and nutrition, while losses in key commodity crops such as fruits, nuts, and flowers have major impact ranging from household to national economies. Additionally, the threat of plant pests and diseases are increased by climate

fluctuations causing additional hindrance towards achieving sustainability in agriculture. Therefore, reduction in crop losses will prove to be a major part of boosting agricultural efficiency, and will require significant efforts towards improved management of pathogenic and pest related stresses in plants.

Traditionally, biotic attacks on crops are determined through manual visual inspections based on physiological signatures such as lesions, tumors, wilting, stunted growth, discolorations, and cell death. At that stage, the majority of the damage has already occurred, leaving little to no room for treatments. Alternatively, based on prior knowledge and/or rule of thumb, growers may apply agrochemicals like, pesticides, fungicides, or bactericides to prevent pest and/or phytopathogenic damages, however, the application is not optimized and often the chemicals are used in excess leading to environmental contamination as well as economic stress. Therefore, identifying stress responses in plants in a timely manner is of critical importance with direct impact on yield, food security, agricultural economics, and the environment.

The progress made towards understanding the defense mechanisms in plants, from the moment of coming in contact with a stressor to expressing physiological measures and effects, has paved the way for developing sensing techniques for crop health management to improve the sustainability of agroecosystems. Methodologies enabling early and accurate detection of plant stress due to pathogens and pests provide a way for optimal deployment of countermeasures for reducing of losses in yield. Our group has been pursuing agriculture sensor design for soil [5–17] and plant health [18–26], modeling for soil moisture/nutrients and plant growth dynamics [27,28], and decision-making for irrigation and fertilization for over a decade [27,29].

This article aims to present the current state of the sensing methodologies applied towards stress detection in plants caused by pests/insects and phytopathogens, while discussing the gap in technologies which may, in the future, help reduce crop yield losses bringing us closer to achieving sustainability in agriculture. Figure 1 shows an outline of the methodologies discussed in this article. The paper is organized into several sections: Section 1 provides the introduction, whereas Section 2 addresses the question: how do plants respond to stress? Section 3 discusses sensing methods developed for detecting pathogenic stresses in plants; Section 4 describes the methods applied towards the determination of pest attacks in crops; Section 5 discusses methods for volatile organic compound emissions as an indicator of biotic stress; Section 6 focuses on the application of active remote sensing technologies for detecting biotic stress in plants. Section 7 presents discussion and conclusion while Section 8 focuses on the future of biotic stress monitoring in plants.

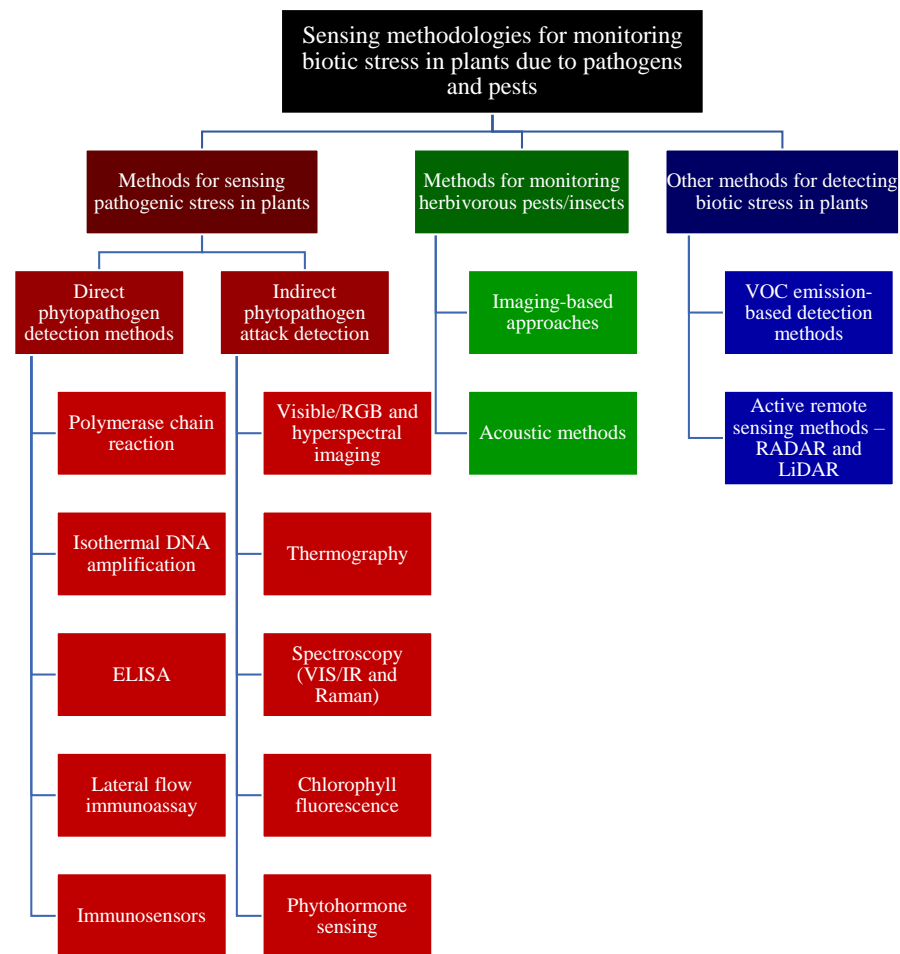


Figure 1. An outline of the plant biotic stress sensing methodologies discussed in this article.

2. How do Plants Respond to Stress?

Plants are constantly exposed to the ever-varying elements of nature, and have evolved unique mechanisms for detecting and responding to different types of stress. *Stress* in plants can be defined as any unfavorable condition that causes significant disruptions in the plant's "normal" metabolism, growth, and development processes. Stress can be caused by *biotic* or living agents such as, fungi, bacteria, oomycetes, viruses, pests, or by *abiotic* or environmental factors such as, drought, nutrient deficiency, extreme temperatures, radiation, and pollution. As compared to animals, plants have evolved a less intricate but effective immune system. Plant defenses can be broadly classified into two categories: (i) *physical* defenses that include preformed barriers like, bark, plant cell walls, waxy cuticles, trichomes, thorns, spines, and thicker leaves, and (ii) *induced* defenses such as, accumulation of signaling hormones, production of toxic chemicals, release of attacker deterring volatile organic compounds, and deliberate cell suicide. Defense responses in plants are tightly regulated by complex signaling pathways depending on stimulus perception as there is high energy cost and nutrient requirements associated with them.

This article focuses primarily on the sensing methodologies developed in agriculture for monitoring diseases and stress caused due to *biotic* aggressors—pathogens and pests. A recent article by our group provided a comprehensive survey of soil moisture and nutrient sensing that cover the key abiotic sources of stress [19]. This section presents an overview of the responses of biotic stresses in plants that enables the development of technologies to detect them. Figure 2 presents a brief overview of the recognition mechanisms against phytopathogen and pest/insect attacks in plants resulting in the onset of induced defenses and hormone signaling.

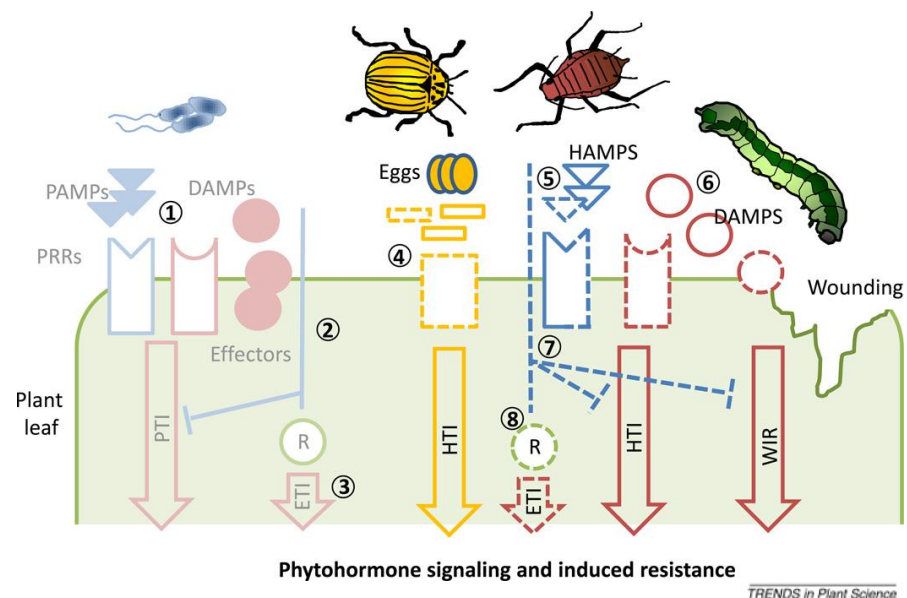


Figure 2. Recognition mechanisms of biotic stresses due to phytopathogens and pests. Reprinted from [30], Copyright (2012), with permission from Elsevier. MAMPs, PAMPs, DAMPs, and HAMPs refer to microbe-, pathogen-, damage-, and herbivore-associated molecular patterns, respectively; PRRs are pattern recognition receptors; PTI/ETI and HTI refer to PAMP/effector- and herbivore-triggered immunity, respectively; WIR refers to wound-induced resistance; uncharacterized elements are indicated by broken lines.

2.1. Responses against Phytopathogens

Phytopathogens can be divided into three main categories: (i) *biotrophs*, these pathogens feed silently on the living tissue, extracting nutrients gradually while keeping their host plants alive and functioning; (ii) *necrotrophs* overwhelm the plants defenses by producing toxins and tissue-degrading enzymes, feeding on the dead tissue resulting in rapid loss of nutrients from the host; (iii) *hemibiotrophs*, these pathogens act as biotrophic during initial stages of infection, but turn necrotrophic in later stages of the disease [31]. Subsequent to the physical defense barriers, the next line of active resistance comes from the induced *innate immunity* in plants, also known as *basal resistance*. This occurs at the plant cell surface when pathogen- or microbe-associated molecular patterns (PAMPs or MAMPs) such as, specific proteins, liposaccharides, β -glucans, chitin, peptidoglycans and bacterial flagellin, which are commonly found on the microbes, are detected on the host (plant) cell surface through special trans-membrane proteins called pattern recognition receptors (PRRs) [32,33]. PAMP/effector-triggered immunity (PTI/ETI) is considered to be responsible for non-host specific resistance, occurring at or above the species level [34]. Refs. [32,35,36] studied physiological responses, local to attack-site, under PTI/ETI that include increase in Ca^{2+} concentration, plant cell membrane adaptations, production of reactive oxygen species (ROS), and cell wall fortification.

Adapted pathogens can tackle PTI by injecting *effector* molecules, which are microbe-produced proteins/toxins, that can suppress the function of host immune regulators, promoting pathogen virulence. For example, *Pseudomonas syringae* (*P. syringae*) strains contain dozens of such effectors like, AvrPto1 of *P. syringae*, that have been shown to promote pathogen virulence by suppressing immune-related proteins in tomato plant [32]. In response, plants have developed intracellular immune receptors known as resistance (R) proteins that can activate *effector-triggered immunity*. This second level of immunity is commonly characterized by *hypersensitive response* (HR) which is typically associated with programmed cell death at/near the infection site to prevent further pathogen transport to other parts of the plant, as well as the production of antimicrobial molecules. In contrast to the PAMP-triggered immunity (PTI), effector-triggered immunity (ETI) is specific to a

microbe. Fungi, bacteria, viruses, and microscopic nematodes are all subject to induction of HR. A local HR response can also trigger immunity against future infections for an extended period of time, this phenomenon has been termed as, *systemic acquired resistance* (SAR) by A. Frank Ross in 1961, who discovered it for tobacco plants infected with tobacco mosaic virus (TMV) [37]. SAR represents a long-lasting, broad spectrum immune response, where resources are mobilized throughout the plant for taking quick measures in case of any future attacks.

Moving immune signals play a critical role in SAR, and understanding the signaling mechanisms related to SAR is a major area of research. These signals are generated in the infected tissue and are rapidly transported to other parts of the plant. The onset of SAR is accompanied by the accumulation of signaling plant hormones or phytohormones, major among which include, salicylic acid (SA), jasmonic acid (JA), ethylene (ET), and Abscisic acid (ABA) [32,38]. In general, it has been established that phytohormone signaling mediated by ABA promotes abiotic stress tolerance while SA promotes biotic stress tolerance [39]. Additionally, SA mediated responses have been linked primarily with biotrophic phytopathogen attacks whereas JA/ET hormone signaling have been associated with necrotrophic phytopathogens and pest attacks [40,41]. Moreover, molecular crosstalk exists between the different hormone signaling mechanisms, where under abiotic stress, ABA-based defenses suppress signaling of biotic stress-related phytohormones [39]. Furthermore, increasing evidence indicates mutually antagonistic relation between SA- and JA/ET-mediated pathways [38,41].

2.2. Responses against Herbivorous Pests/Insects

Plants have evolved specific defense mechanisms to recognize and respond to herbivorous pest/insect attacks which include physical barriers such as waxy cuticle, trichomes (often toxic), spines/thorns, and hardened leaves, plus the induced defenses which are generally triggered by mechanical damage to the plant tissue. Plants can distinguish between general wounding and insect feeding based on the presence of elicitors contained in the saliva of insects [31]. Similar to PTI/ETI in case of phytopathogens, herbivore-associated molecular patterns (HAMPs) which are insect-derived compounds are recognized by receptors on the attack site which leads to herbivore-triggered immunity (HTI). Additionally, wounding leads to the release of damage-associated molecular patterns (DAMPs) resulting in wound-induced resistance (WIR) [30,34]. Pests not only cause physical damage to the plant tissue but also act as vectors for diseases while providing entry points for carrier phytopathogens through wounds. Clear identification of HTI and WIR trigger mechanisms is an active area of research, where several studies have been conducted to distinguish HTI (based on insect secretions) and WIR (self triggered) [30]. HTI/WIR responses include increased calcium signaling, and release of ROS and deterring chemicals/toxins; their detailed roles and mechanisms are described in [36].

Most herbivores inflict much greater cell damage than simple phloem feeders, and activate hormone signaling, where resistance traits are induced by largely JA/ET pathways. Systemic signaling via the vascular system induces defense throughout the plant, similar to the phenomenon of induced SAR after pathogen attack. The broad spectrum of defense responses induced by hormone signaling pathways include antioxidative enzymes, proteinase inhibitors (PIs), and released volatile organic compounds (VOCs), including monoterpenoids, sesquiterpenoids, and homoterpenoids that have been known to repel harmful insects and attract beneficial predators [31,36].

3. Methodologies for Sensing Pathogenic Fragment/Stress in Plants

Sensing methodologies for pathogenic disease detection in plants can be classified into two broad categories: Direct versus indirect methods. Table 1 presents a general qualitative comparison between the key microbial stress detection methods in plants. Detailed comparisons wherever necessary among various methods are presented in the subsequent sections.

Table 1. Brief comparison of the direct sensing methods discussed in this article for monitoring phytopathogenic stress in plants.

Direct Phytopathogen Detection Methods				
Sensing Method	Brief Description	Performance (Sensitivity)	Strengths	Limitations
Polymerase chain reaction (PCR)	Pathogens are identified by selective DNA amplification using specific primers and thermal cycling.	1–100 fg/ μ L [42]	Highly selective, reliable and sensitive, cost effective, well established.	Extensive sample preparation and precise thermal cycling required, non-portable.
Isothermal DNA amplification	Utilizes special primers only without thermal cycling for DNA amplification.	0.01–1 pg/ μ L [43,44]	Selective, reliable, thermal cycling not required making operation simpler.	Complex primer needs for successful testing, elaborate sampling and testing procedure.
ELISA	Detection mechanism consists of affinity-based interaction between antigen (pathogen-specific protein) and antibody.	1–100 fg/ μ L [45]	Easy to use, suitable for high throughput testing, and particularly useful for detecting viral antigens	Time consuming, elaborate sample preparation and labeling (antigen extraction) maybe required.
Lateral flow immunoassay	Based on colorimetric detection of the formation of antigen–antibody complex.	0.1–1 pg/ μ L [46–48]	Portable, inexpensive and easy to use.	Qualitative-only, sample preparation is often required to extract antigen proteins.
Immunosensors	Identification of the antigen–antibody complexes using various transduction mechanisms.	0.1–10 pg/ μ L [49,50]	Highly portable, quantitative, easy to use	Variability in operation.

ELISA = Enzyme-linked immunosorbent assay.

3.1. Direct Pathogen Detection Methods

Direct detection methods refer to the techniques where the pathogens are identified directly as a way of sensing for diseases. These methods are most commonly used in the laboratory setting for high-throughput analysis, but have also recently been reported for use in portable and/or in-field sensing applications. Direct phytopathogen detection methods discussed in this article can be largely classified into two categories: *nucleic acid-based* methods, and *serological/immunological* methods.

Nucleic acid-based methods use various forms of deoxyribonucleic acid or ribonucleic acid (DNA/RNA) recognition techniques to identify the disease causing micro-organisms. In general, these techniques work by selective amplification and subsequent detection of the target DNA. Common amplification choice in nucleic acid based methods include polymerase chain reaction (PCR), recombinase polymerase amplification (RPA), loop-mediated isothermal amplification (LAMP), nucleic acid sequence-based amplification (NASBA), and helicase-dependent amplification (HDA). Among these, PCR is the most established method and requires thermal cycling for DNA/RNA amplification whereas RPA, LAMP, NASBA, and HDA are contemporary methods that operate under isothermal conditions while using specific enzyme cocktails for DNA/RNA amplification.

Serological/immunological methods rely on identifying pathogen specific bio-molecules (antigens). The immune reaction in plants (host) is triggered based on the recognition of an invader through the ability of specific host proteins (antibodies) to bind to unique pathogen proteins (antigens). Following the similar principle of recognition,

serological methods operate by extracting serum from the infected plant tissue and testing for antigens related to pathogens using specific antibodies. Key serological methods include enzyme-linked immunosorbent assay (ELISA), lateral flow immunoassays, and antibody-based biosensors/immunosensors.

3.1.1. PCR-Based Methods

PCR is a versatile tool that was developed by Kerry B. Mullis for which he was awarded the Nobel prize in 1993 [51]. It has since been used extensively in diagnostics to detect diseases through pathogen identification by rapidly synthesizing millions of copies of specific DNA sequences. As shown in Figure 3, the process begins by separating the extracted double-stranded DNA (dsDNA) into two single-stranded DNA (ssDNA) molecules by heating to 95 °C, the temperature is then reduced to 40–65 °C allowing for the binding of the primers at each end of the target ssDNA's region to be amplified [52]. The primers are short pieces of ssDNA which bind specifically to the target DNA sequence by complementary base pairing. Finally, the complementary strand to the target sequence in the ssDNA sandwiched between the primers is generated at around 72 °C using the thermostable enzyme, DNA polymerase, and deoxyribonucleoside triphosphates (dNTPs). In this way after each cycle the number of copies of the target DNA sequence are doubled, and in a few hours, millions of such copies can be generated. The overall process requires only a few ingredients (DNA, buffer, dNTPs, primers and DNA polymerase) and a programmable heating block forming the majority of a PCR machine.

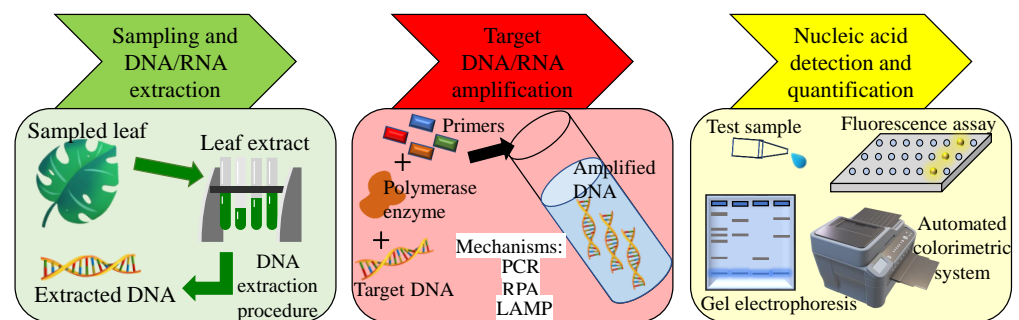


Figure 3. General steps involved in nucleic acid amplification-based phytopathogen detection.

The amplified DNA can be detected using methods like gel electrophoresis (most commonly used), colorimetric assays, and fluorometric assays. Over time, several advances have been made to the basic PCR such as, (i) reverse-transcriptase PCR (RT-PCR) that extends the application for replicating RNA by reverse transcribing the RNA templates with the enzyme reverse transcriptase to produce complementary DNA, (ii) nested-PCR (n-PCR) that improves the sensitivity and specificity through a second PCR reaction using primers that recognize a region within the PCR product amplified by the first set [52], (iii) multiplexed PCR (m-PCR) where several PCR primers are used in the same reaction to identify multiple pathogens, and (iv) quantitative real-time PCR (qPCR). Standard PCR is not inherently quantitative and may not correctly represent the concentration of the target DNA originally present, however, qPCR has emerged as a successful technique widely used in laboratory-based as well as portable applications for pathogen detection. This technique monitors the amplification of the target DNA in real-time via a target-specific fluorescent signal which can also be used for quantification.

Sample preparation and DNA extraction for PCR molecular analysis are critical steps that require precise procedures for reproducible results. Figure 4 shows a comparison between the standard conventional DNA extraction techniques versus a recently reported micro-needle-based approach. According to the extracted genomes, RNA, ssDNA or dsDNA, specific protocols for PCR analysis have been designed for use in commercial as well as research applications [53,54]. Some of the commonly used commercially available

PCR kits include, DNeasy and RNeasy Plant System from Qiagen, Ultra Clean Plant RNA, DNA isolation kits from MoBio, and the Easy-DNA Extraction kit and Extract-N-Amp Plant PCR kit from Sigma Aldrich [55]. In addition to the specific sample preparation and DNA/RNA extraction protocols, accurate design of primers, oligonucleotides, and probes also play a critical role in molecular detection methods for sensing plant pathogens. Functional target sequences can be found using the databases such as *GenBank*[®] nucleotide sequence search program provided by the National Center for Biotechnology Information (NCBI, Bethesda, MD, USA).

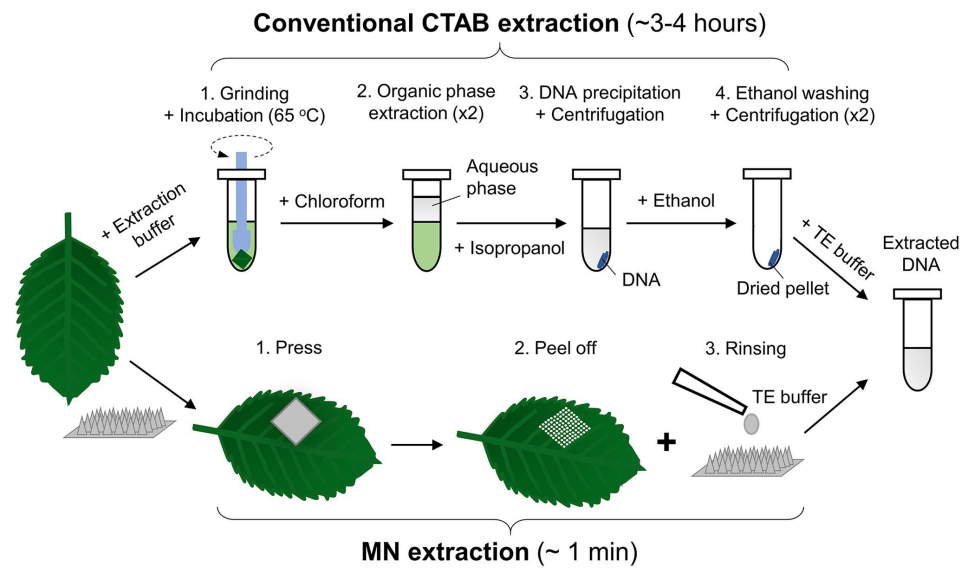


Figure 4. DNA extraction procedures for nucleic acid-based methods, a comparison between conventional method (cetyltrimethylammonium bromide; CTAB) and a micro-needle (MN)-based approach. Reprinted with permission from [56]. Copyright (2019) American Chemical Society.

PCR-based methods are among the most commonly used techniques in plant pathology in laboratory settings, but face several challenges for portable operation such as, sample preparation, DNA extraction, portable temperature control system, and fouling due to exposure to variable surrounding conditions. Despite these challenges, several PCR-based techniques, portable or otherwise, for direct disease detection in plants have been reported in the literature with key recent works described here.

A complete real-time microchip PCR system composed of a thin-film heater integrated PCR reaction chamber, a compact fluorescence detector for detecting amplified DNA, and a microcontroller that controls the entire operation for portable plant disease diagnosis was reported in [57]. The disposable microchip requiring 8 μL sample volume was made of two glass slides, where the bottom slide has a stationary reaction chamber holding the PCR sample and the top slide has a thin film heater (patterned Cr/Au deposited on glass using e-beam evaporation). An optical set-up was used for real-time PCR system based on the detection of fluorescence dyes that intercalate with DNA, where fluorescent intensity is proportional to the amount of amplified DNA. The dye is excited with light emitted from an LED, and the emission light passing through series of filters and lenses is detected through a photomultiplier tube. The entire system was $25 \times 16 \times 8 \text{ cm}^3$ in size and 843 g in weight, and consumed 110 mAh of power for each PCR run. The developed system was tested using prepared samples containing *Fusarium* species and *Pseudomonas* species as fungal and bacterial phytopathogens, respectively. DNA extraction was performed using a commercial kit (Plant/Fungi DNA Isolation Kit, Norgen Biotek Corp., Thorold, ON, Canada). The sensor exhibited a detection limit of 5 ng/8 μL sample with a 100% success rate, validated using gel electrophoresis.

A droplet digital PCR (ddPCR) sensing system for detecting common bunt disease (caused by *Tilletia laevis*) in wheat was reported in [42]. The ddPCR exhibited superior detection limit of 30 fg/ μL as compared to qPCR (100 fg/ μL). In case of qPCR, a parameter called quantification cycle (C_q or threshold cycle, C_t) is defined which represents the PCR cycle number after which the real signal from the sample becomes detectable against background fluorescence. Hence, C_q controls the limit of detection in a given qPCR system as shown in the Figure 5. Whereas in case of ddPCR, the sample (a few μL) is divided into hundreds of nL droplets suspended in an oil using a droplet generator, and after thermal cycling, the droplets are classified as positive or negative based on the fluorescence response recorded using a droplet reader. In the presented work, a ddPCR system (QX200, Bio-Rad, Hercules, CA, USA) was used for generating and analyzing droplets, where 40 μL of PCR master mix (containing primers, target DNA, and ddPCR probes) and 70 μL of droplet-generating oil (186-3005, Bio-Rad, Hercules, CA, USA) was used as inputs to the ddPCR system.

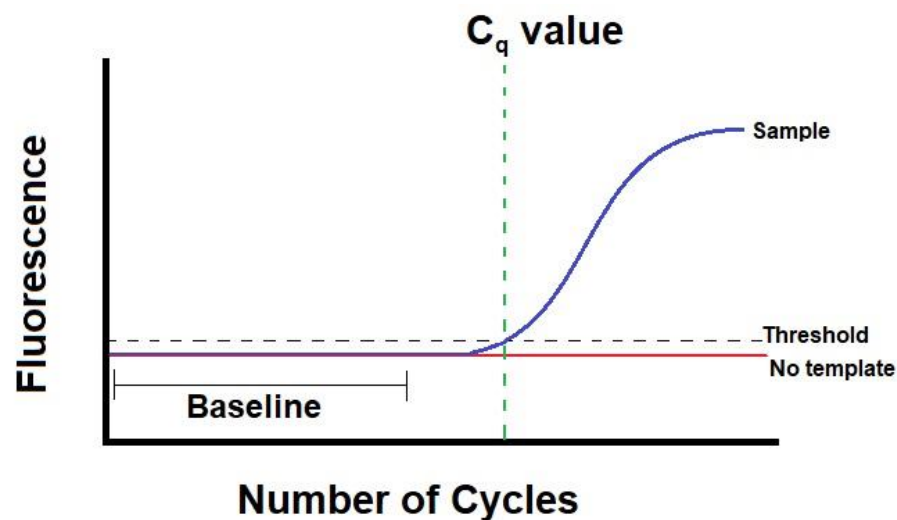


Figure 5. C_q value on a quantitative real-time PCR amplification curve [58].

A micro-needle (MN) patch-based DNA extraction method was reported in [56] to enable a truly portable PCR-based plant disease detection system. qPCR was used to detect late blight (caused by *Phytophthora infestans*) disease in tomato, where the MN extraction achieved 100% detection rate when compared to the conventional gold standard cetyltrimethylammonium bromide (CTAB)-based DNA extraction method. The leaf samples were collected three days after inoculation. The MN-based method significantly shortened the time of plant DNA extraction from ~ 3 to 4 h in a conventional method to around 1 min as shown in Figure 4, while overcoming the requirement for using bulky and expensive equipment.

In addition to the aforementioned works, several other efforts related to PCR-based phytopathogen detection have been reported in the past decade, such as a multiplex RT-PCR (mRT-PCR) method for simultaneous detection of five grapevine viroids [59], the use of qPCR for the detection and quantification of filamentous fungi and oomycetes within host tissue, soil, air, and water [60], a qPCR assay for the detection and quantification of *Verticillium dahliae* in spinach seed resulting in reliable measurements with sensitivity limit of about 1 infected seed per 100 [61], and an on-site system for detecting soil-borne pathogen (*Spongospora subterranea*) that causes Powdery scab in potato using magnetic bead-based nucleic acid extraction, and portable qPCR (fluorogenic probe-based assay) [62].

Alternative nucleic acid-based methods overcoming the need for precise temperature cycling in PCR have also been developed, key among which include RPA and LAMP-based methods which are overviewed next.

3.1.2. Isothermal Nucleic Acid Amplification-Based Methods

RPA is an isothermal nucleic acid amplification method which does not require thermal-cycling like in PCR-based methods and can generally be performed at a constant temperature between 25 to 42 °C, achieving amplification in as little as 15 min [63]. RPA mechanism starts when a recombinase protein binds to the primer forming recombinase-primer complex which interrogates dsDNA seeking homologous sequence and promotes strand invasion by the primer at the cognate site. Next, to prevent the ejection of the inserted primer by branch migration, the displaced DNA strand is stabilized by the ssDNA-binding protein. Finally, the recombinase disassembles and a strand-displacing DNA-polymerase binds to the end of the primer to elongate it in the presence of dNTPs [64]. Cyclic repetition of this process results in the exponential amplification of the target DNA sequence.

An isothermal amplification of target pathogen DNA sequences by RPA followed by gold nanoparticle-based electrochemical assessment with differential pulse voltammetry (DPV) was reported in [65]. The RPA coupled with gold nanoparticles (AuNP) electrochemical (EC) biosensor was developed to detect the pathogen *Pseudomonas syringae* in Arabidopsis plant. The DNA was extracted from plant samples using the solid phase reversible immobilization (SPRI) method, followed by mixing with the primers for amplification. After amplification, the resulting amplicons, containing a barcode sequence on one end and biotin on the other, were hybridized to AuNPs using DNA probes complementary to the barcode sequence. Streptavidin magnetic beads were then used to enrich for AuNPs/DNA/biotin products. The magnetic beads/AuNPs/DNA/biotin products were heated to denature the dsDNA amplicons and to release any bound AuNPs into solution, where the electrochemical reduction of Au (III) to Au (0) was measured with DPV. The data indicated that RPA-EC assay (214 pM) was 100 times more sensitive than PCR-gel electrophoresis (21,400 pM).

In another work, a rapid, equipment-free detection of *Phytophthora capsici* (oomycetes that infect multiple plant species including *Cucurbitaceae*, *Solanaceae*, and *Leguminosae*) using lateral flow strip-based RPA (LF-RPA) assay was developed [66]. A 30 s equipment-free DNA extraction method using cellulose-based dipstick to rapidly capture nucleic acids was employed. The dipstick method was proposed in [67], where a cellulose strip coated with nucleic acid binding proteins is dipped in homogenized tissue sample and then washed in buffer resulting in a rapid and simple DNA extraction procedure. It was determined that 10 to 20 min of DNA amplification time at 40 °C is sufficient for LF strip-based detection. LF strips enable detection of biotin- and 6-carboxy-fluorescein (FAM)-labeled amplicons produced during RPA. The primers used in DNA amplification were labeled with biotin and fluorescence probes (like FAM) that bind to LF strips and causes visible changes. The developed method exhibited a detection limit of 10 pg of genomic DNA.

In addition to the studies described above, several other recent works have been reported using RPA-based phytopathogen detection including (i) the design of four separate RPA assays for the detection of four pathogens, *Xanthomonas gardneri*, *X. euvesicatoria*, *X. perforans*, and *X. vesicatoria* that cause bacterial spot of tomato [68]; (ii) the detection of *bean golden yellow mosaic virus*, *tomato mottle virus*, and *tomato yellow leaf curl virus* (TYLCV) in tomato and beans [63], where RPA was able to detect 9.6 pg and PCR was able to detect 9.6 fg of purified TYLCV DNA indicating the sensitivity of PCR (however, PCR was unable to generate visible amplicons during gel electrophoresis unlike RPA which produced results even with crude sample extraction); (iii) the detection of plum pox virus (a disease causing virus in stone fruit trees) using a commercial reverse transcription-RPA (RT-RPA) platform called AmplifyRP, where the whole process from sample preparation to results took about 20 min and provided better sensitivity as compared to ELISA-based detection [69]; (iv) the rapid detection of *Cucumber green mottle mosaic virus* by RT-RPA, where a detection limit of 0.5 pg of total viral RNA was observed [70]; (v) the detection of *Little cherry virus 2* using RT-RPA, where a crude sample extraction method involving homogenization of leaf tissue in a mesh bag with an extraction buffer was employed [71], and in which the incubation for the RT-RPA was performed at 39 °C for 15 min before visual detection using LF strips.

LAMP is another prominent isothermal DNA amplification technique applied towards phytopathogen detection. In LAMP, four to six target-specific primers (categorized into forward and reverse primers) each consisting of a 3' and a 5' region and DNA polymerase enzyme for strand displacement are required to generate products. Amplification begins by denaturation of the dsDNA into ssDNA after which a forward inner primer binds to its respective region on the ssDNA and the complementary bases are generated by the DNA polymerase. Another different forward primer then binds to target upstream (in 5' to 3' direction) of the first primer's site and displaces the strand formed by the first primer by synthesizing complementary DNA (cDNA). The reverse inner primer now binds to the newly released strand at its respective target and initiates reverse (in 3' to 5' direction) DNA synthesis using the polymerase enzyme, and then another reverse primer binds to target downstream of the first reverse primer's site and displaces the strand formed by the first reverse primer by synthesizing cDNA. The strand synthesized by the action of the two forward and reverse primers contains two complementary regions which bind together to form a dumbbell shape with 2 loops [72,73]. This dumbbell structure forms the basis of cycling phase. LAMP-based amplification takes place at a constant temperature around 65 °C and is faster than PCR taking about 30 min for detectable results [43,74].

Several recent LAMP-based phytopathogen detection systems are reported in the literature including (i) the detection of root infecting fungi in turfgrasses [74]; (ii) the detection of quarantine plant pathogens such as *Xylella fastidiosa*, *Ceratocystis platani*, and *Phytophthora ramorum*, three of the most devastating pathogens of trees and ornamental plants in Europe and North America, where a detection limit of 0.02 pg/μL of DNA was achieved [43]; (iii) a comparative study using LAMP and ddPCR for detecting *Phytophthora infestans* which causes potato late blight [44]. It was observed that ddPCR exhibited the lowest detection limit of 100 fg/μL whereas with SYBR green LAMP-based method a detection limit of 1 pg/μL was observed.

Isothermal nucleic acid amplification-based techniques for phytopathogen detection have gained momentum in the recent years owing to their simpler equipment needs, lower cost, faster operation, and better potential for in-field or portable operation as compared to conventional PCR-based methods.

In general, utilizing the power of DNA amplification technology requires developing specific DNA primers and a reliable assay protocol but offers excellent selectivity and reliability which has made them a standard laboratory technique for pathogen identification and quantification. However, there are some limitations associated with the techniques such as large time consumption, requirement for sophisticated equipment, elaborate sample preparation, and expert training. Continuous efforts are being directed towards making the techniques portable, easy to use, economical, and developing new standard procedures/protocols for fast reliable measurements.

3.1.3. Serological/Immunological Methods

ELISA is among the most widely used serological techniques in disease diagnostics for both animals and plants. It is a fairly mature technology with several phytopathogen identification kits available commercially [75,76]. The basic principle of ELISA involves first, the immobilization of the antigen (target protein in the sample) to be detected onto a solid surface through adsorption. During this step, the antigen can directly be adsorbed on the surface, or alternatively, a capture antibody (or primary antibody), previously adsorbed on the surface, can be used to immobilize the antigen. Then, the surface is rinsed to remove unadsorbed/excess material. Next, the secondary enzyme-linked antibodies are introduced that bind to the target antigen, followed by the addition of the enzyme's substrate or fluorescent dye to detect the antigens through a change in color. Only in the presence of specific antigen-antibody interaction is the signal generated. A colorimeter is often used to measure the intensity of the color change and calculate the concentration of the antigen precisely. In addition to the basic ELISA mechanism (direct ELISA), other variants have also been

developed such as indirect ELISA, sandwich ELISA and competitive ELISA [77] along with multiplexed phytopathogen detection [45].

Lateral flow immunoassay (LFIA) is another major serological/immunological technique developed for detecting antigens. LFIA is a low-cost, easy-to-use paper-based platform, where a liquid sample containing the analyte of interest (antigen) moves under the effect of capillary action through various zones of polymeric strips impregnated with antibody molecules followed by colored or fluorescent particles (most commonly colloidal gold and latex microspheres) that label the antibody–antigen complex, if present (see Figure 6). The sample together then migrates to the detection zone where specific immobilized bio-molecules interact with the conjugated antigen–antibody complex and produces a recognition signal in form of a visual color change [78]. In many cases, a control line is present after the detection zone/test line which indicates proper liquid flow through the strip. In contrast to ELISA-based detection, LFIA-based sensors are more suitable for in-field or portable applications but are often less sensitive and exhibit inferior quantitative capability.

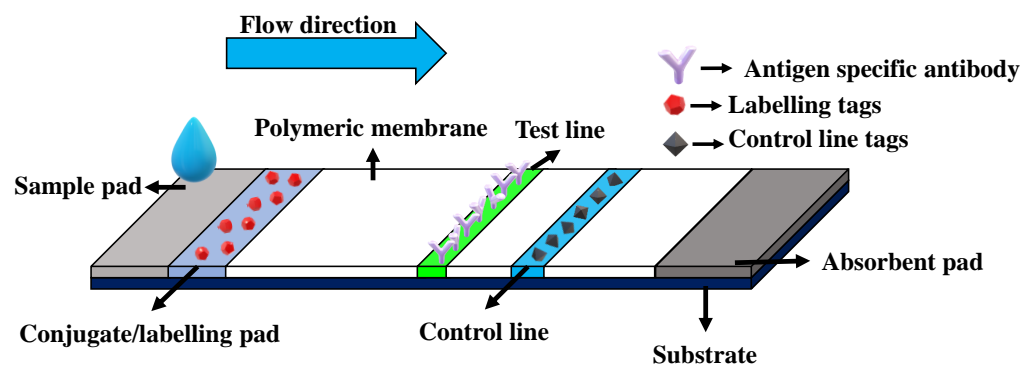


Figure 6. Schematic of a general lateral flow immunoassay-based device.

Several LFIA-based sensors have been reported for phytopathogen detection, where some key recent studies include (i) a double enhanced LFIA containing magnetic and gold nanoparticles (MNPs and AuNPs) for the detection of potato virus X (PVX; genus *Potexvirus*) [79], where the concentration of analyte was increased in the samples using conjugates of MNPs with specific antibodies and visibility of the label was increased through MNP aggregation caused by AuNPs. A detection limit of 0.25 ng/mL was observed as compared to 8 ng/mL in case of non-enhanced LFIA with operation time of 10 to 15 min; (ii) a multiplex LFIA for the simultaneous determination of three mycotoxins (toxic metabolites produced by fungi) in corn, rice, and peanut [80]. Here the LFIA strip consisted of three test lines, one for each mycotoxin, and exhibited a detection limit of about 10 µg/kg to 50 µg/kg; (iii) another multiplex LFIA-based sensor for mycotoxin (*aflatoxin B1*, *zearalenone* and *deoxynivalenol*) determination in cereal crops (maize and wheat samples) with a visual detection limit of 0.03 to 10 µg/kg [47]; (iv) an Ag-enhanced LFIA for the detection of potato leafroll virus [46], where the Ag enhancement is based on the reduction of Ag ions on the surface of AuNP (used for labeling) resulting in a significant increase of initial AuNP-caused coloration. A detection limit of 0.2 ng/mL and an operation time of 15 min was observed; (v) an LFIA device for detecting ochratoxin A (a mycotoxin) in wines and grapes, where a gold-silver enhancement scheme was implemented. A detection limit of 0.9 µg/L was achieved with an assay time of 10 min [48].

Immunosensors or antibody-based biosensors can also be categorised under serological techniques, where the general detection mechanism involves the study of antigen–antibody interactions and their quantification using electrochemical (EC), optical, and spectroscopic methods. The application of immunosensors is a growing area of study in plant pathology as they provide quantitative information while exhibiting potential for rapid, portable, and low cost analysis. A few key recent works covering the application of immunosensors in plant pathology are discussed here.

A label-free electrochemical (EC) immunosensor based on electro-deposited Prussian blue (PB) and AuNPs for the detection of citrus bacterial canker disease (caused by *Xanthomonas citri* subsp. *citri*; Xcc) based on the directly recognizing the effector protein PthA was developed in [81]. The sensor fabrication involved sequential electro-deposition of PB and AuNPs on multiwall carbon nanotubes (MWCNTs)-ionic liquid nanocomposite modified glassy carbon electrode. After immobilization of the anti-PthA antibody and blocking with bovine serum albumin (BSA) protein, the immunosensor was used for determination of different concentrations of PthA antigen under the optimal conditions. The developed sensor was characterized using cyclic voltammetry (CV) and EC-impedance spectroscopy (EIS), where a linear dynamic range of 0.1 to 50 nM with a detection limit of 0.028 nM was achieved.

An EC immunosensor to determine zearalenone (ZEA; a mycotoxin) in maize using carbon screen printed electrodes modified with MW-CNTs/polyethyleneimine/AuNPs was presented in [82]. Anti-ZEA poly-clonal antibodies were immobilized on the AuNPs, where the immunoassay was based on a direct competitive assay between ZEA in maize samples and ZEA labeled with horseradish peroxidase enzyme (ZEA-HRP). The EC sensor was characterized using amperometry where first, H₂O₂ (added to the sample solution) was reduced to H₂O by HRP, and then the remaining H₂O₂ was reduced electrochemically leading to an EC signal proportional to the antigen ZEA in the sample. The developed sensor exhibited a linear detection range of 10⁻⁴ to 10⁻¹ ng/mL with a detection limit of 0.15 pg/mL.

Gold nano-rods (AuNRs)-based fiber optic particle plasmon resonance (PPR) immunosensors for the label-free detection of orchid viruses, *Cymbidium mosaic virus* (CymMV), and *Odontoglossum ringspot virus* (ORSV), was presented in [49]. AuNRs were synthesized by seed-mediated growth method and immobilized on the fiber core followed by the functionalization of antibodies for CymMV or ORSV via a mixed self-assembled monolayer of alkanethiols using the reagents, 1-ethyl-3-(3-dimethylamino-propyl) carbodiimide hydrochloride, and N-hydroxysuccinimide (EDC/NHS). The principle of operation was based on the localized evanescent field absorption by the AuNRs upon biomolecular binding, resulting in decreased transmission intensity measured at the distal end of the fiber. Using the developed sensor, a detection limits of 48 pg/mL and 42 pg/mL for CymMV and ORSV, respectively, were achieved.

A bioelectronic plum pox virus (PPV) biosensor based on a electrolyte-gated organic field effect transistor (EGOFET) was reported in [50], where a poly-crystalline gold wire gate electrode was functionalized with anti-PPV. The immobilization procedure involved first, covalent binding of a (sub)monolayer of recombinant Protein G onto the gold surface followed by anti-PPV antibodies (Abs) adsorption. Additionally, a (11-Mercaptoundecyl)tri(ethylene glycol), OEG, self-assembled monolayer was deposited to avoid non-specific adsorption to the gold surface spots not covered by the ProteinG/Ab. EGOFET was tested by incubating the functionalized gate ex-situ, in solutions containing increasing PPV and recording the transfer characteristics in phosphate buffer saline (PBS) 50 mM, pH 7.4 to extract transistor parameters in linear regime. A calibration curve based on transconductance changes as a function of PPV was constructed, where a detection limit of 180 pg/mL and a dynamic linear range of 5 ng/mL to 50 µg/mL was observed.

In addition to the above-described works, several other recent immunosensing studies have been reported in the literature including: (i) an EC immunoassay for detecting *Pantoea stewartii* sbsp. *stewartii*-NCPB 449 (PSS) in maize using AuNPs and HRP for dual signal amplification, where HRP-labeled anti-PSS antibodies (D-Ab-HRP) were attached to the surface of AuNPs and a sandwich immunosensor of capture anti-PSS antibody (C-Ab), PSS, and D-Ab-HRP was established. A linear detection range of 2×10^7 to 4×10^4 cfu/mL with a detection limit of 7.8×10^3 cfu/mL was achieved [83]; (ii) a lab-on-a-chip platform consisting of an array of gold inter-digitated electrodes functionalized with EDC/NHS/anti-*Pectobacterium atrosepticum* antibodies for monitoring blackleg and soft rot disease of potato. EIS measurements were conducted for quantification, where the measured impedance was directly proportional to the antigen concentration [84]. A detection limit of 10^4 cfu/mL was observed; (iii) an SPR-based biosensor for the detection of maize chlorotic mottle virus (MCMV), where 11-Mercaptoundecanoic acid was applied on a gold surface to form a self-assembled monolayer, and a layer of anti-MCMV antibody was crosslinked on the surface using EDC/NHS-based linkage [85].

Overall, serological/immunological methods are uniquely suited for large-scale testing and operate by detecting pathogen-specific proteins. The key advantages of the method includes good selectivity, fast operation, low-cost, and better potential for in-situ testing as compared to nucleic acid amplification-based methods. However, serological methods generally exhibit poorer detection limit and specificity in comparison with nucleic acid amplification-based techniques, while still providing quantitative results.

3.2. Indirect Phytopathogen Detection Methods

Indirect detection methods refer to techniques where the plant's responses to the pathogenic stress are identified as an indicator of the disease. The stress responses may include morphological and/or physiological changes such as variations in the tissue temperature, color, transpiration rate, and accumulation of metabolites and hormones. Key indirect methods for detecting phytopathogenic stress in plants discussed here include imaging-based techniques such as visible/RGB (red, green, and blue)-imaging, hyperspectral imaging, and thermography; visible/infrared (VIS/IR) reflectance/transmittance spectroscopy and Raman spectroscopy; chlorophyll fluorescence-based methods; hormone biosensing methods; VOC monitoring-based methods (discussed in Section 5). Table 2 presents a qualitative comparison of the mentioned indirect phytopathogen detection methods.

Table 2. Brief qualitative comparison of the indirect sensing methods discussed in this article for monitoring phytopathogenic stress in plants.

Indirect Phytopathogen Detection Methods			
Sensing Method	Brief Description	Strengths	Limitations
Visible/RGB imaging	Color-based features are identified and extracted followed by classification using computational algorithms.	Relatively inexpensive hardware (often smartphone-based), non-invasive.	Low scope for pre-symptomatic detection, complex data processing.
Hyperspectral imaging	Spatio-spectral features are extracted in 100s of wavelength bands forming a hypercube followed by data processing to detect symptoms.	Good scope for pre-symptomatic testing, and potential for in-situ automated operation.	Requires sophisticated hardware and complex software.
Thermography	Passive thermal radiation is recorded where local temperature anomalies are used to detect diseases.	Relatively inexpensive, fast response, computationally simple.	Poor specificity, and suitable only for generalized plant health monitoring.

Table 2. Cont.

Indirect Phytopathogen Detection Methods			
Sensing Method	Brief Description	Strengths	Limitations
VIS/IR spectroscopy	Spectral information from ambient light recording and analyzed using a spectroradiometer.	Low-cost, simple set-up, and good general sensitivity.	Poor specificity, no spatial information is recorded making it unsuitable for in-situ operation.
Raman spectroscopy	Detection of disease is based on chemical changes in the plant tissue identified using molecular signature initiated by a laser source.	Easy to use, fast response, and scope for specific disease detection.	Prone to interference from background fluorescence, special hardware is required, difficult application for in-field operation.
Chlorophyll fluorescence	Based on variations (due to stress) in fluorescence that occurs during photosynthesis in the plants.	Provides information about the photosynthetic efficiency that may improve the accuracy when used in conjunction with imaging-based methods.	Time consuming experimental apparatus is required (dark adapting the sample plants).
Phytohormone biosensing	Defense related hormonal signatures are monitored as an indicator of biotic stress in plants	Scope for high specificity, low-cost, fast response, and in-situ application.	Invasive sampling.
VOC emission monitoring	Changes in gaseous emissions from plants are detected as measure of plant health.	Suitable for general plant health monitoring, non-invasive, and scope of automated continuous monitoring.	Challenging experimental set-up, complex sampling and testing, low specificity.
Active remote sensing methods	RADAR and LiDAR technology is used to detect symptomatic morphological changes	Suitable for large-scale non-specific plant health monitoring, LiDAR has scope to detect parameters like CO ₂ and plant water content.	High initial cost, complex sampling and data processing, low specificity.

RADAR = Radio detection and ranging; LiDAR = Light detection and ranging.

3.2.1. Visible/RGB Imaging-Based Methods

Digital photography and imaging have emerged as important tools for crop health monitoring as well as phenotyping applications where various types of imaging techniques have been developed such as, visible/RGB imaging, hyperspectral imaging, thermography, and fluorescence imaging. Table 3 presents a comparison between key recent works on visible/RGB imaging-based crop disease detection. RGB imaging refers to the digital photographic analysis performed in the visible range of the electromagnetic (EM) spectrum, where the captured colored-image can be expressed in the red, green and blue channels. Along with the RGB color space, the image can be transformed into other spaces such as L*a*b* (L* is lightness, a* is red/green value, and b* is blue/yellow value), CMYB (Cyan, Magenta, Yellow, Black), and HSV (hue, saturation, value). Additionally, parameters like texture, gray levels, and shape can also be defined as features for disease symptom detection and identification. In general, the image processing for plant disease detection consists of three main steps (see Figure 7):

- Segmentation of the region of interest.
- Feature extraction.
- Detection and classification.

Table 3. A comparison of the key recent visible/RGB-imaging-based sensing methods for monitoring pathogenic stress in plants.

Sensing Application	Brief Description	Accuracy	Strengths	Limitations	Ref., Year
Cercospora leaf spot and four other diseases in sugar beet	Images taken using a smartphone and processed on servers, a support vector machine (SVM) based classifier with radial basis function (kernel) was employed	68% to 90%	Smartphone-based imaging, multi-disease detection	Poor accuracy for some diseases	[86], 2018
Three wheat diseases: septoria, rust, and tan spot	Hot-spots were first extracted followed by classification using Random-Forest-based statistical inference methods	80%	Images were captured using mobile devices, and a mobile application was developed for fast processing	Moderate specificity, not suitable for early disease detection	[87], 2017
Vineyard disease based on grape leaf images	Color as well as texture based features were extracted, and a histogram comparison based approach was followed for classification	90%	A phone application was developed for generalized plant health monitoring	Lacks specificity in disease detection	[88], 2017
Detecting 26 diseases across 14 crop species	Images taken from PlantVillage dataset and classified using deep learning architectures named: AlexNet and GoogLeNet	over 99% (under specific conditions)	Multi-disease multi-crop system, large diverse dataset, good classification accuracy	Computation-ally intensive, accuracy reduces to 31% for uncontrolled imaging conditions	[89], 2016
Multi-plant multi-disease detection	Color-channel-based pairwise classification approach was applied using a histogram-based structure	58% (average)	Diverse plant and disease database, images largely captured under real field conditions	Poor accuracy, limited dataset	[90], 2016
Powdery mildew and TSWV in bell peppers	A mobile imaging set-up coupled to principle component analysis- or coefficient of variation-based classification system was developed	64.3% (average)	Mobile system suitable for greenhouse operation	Moderate accuracy, in-field testing needed	[91], 2016
Cercospora leaf spot in sugar beet	Robust template matching (to detect and extract features) coupled with pattern recognition using SVM for classification	33% to 83% depending on leaf age	Leaf tracking capability against changes on open field	Poor accuracy in younger leaves, moderate accuracy in older leaves	[92], 2015
Huanglongbing (HLB) disease in citrus plants	Based on the observation that starch in HLB infected leaf rotates the polarization plane of light	97% (average)	Good classification accuracy, simple imaging setup	Cross-validation training method may have caused information loss and/or over-fitting	[93], 2015

TSWV = Tomato spotted wilt virus.

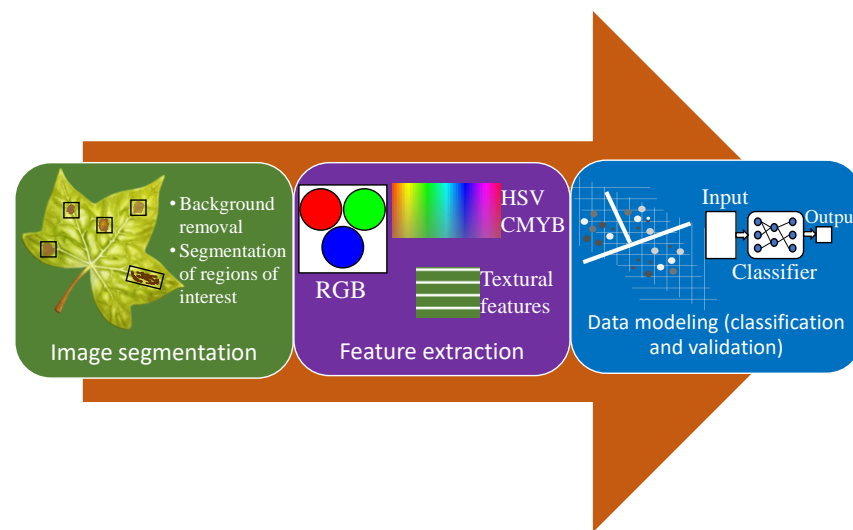


Figure 7. General workflow of visible/RGB imaging-based plant disease detection.

In a recent work, a smartphone-based RGB image processing system was reported to detect and automatically classify five diseases (*Cercospora* leaf spot caused by the fungus *Cercospora beticola*, *Ramularia* leaf spot caused by *Ramularia beticola*, *Phoma* leaf spot caused by *Phoma betae*, Beet rust caused by *Uromyces betae*, and Bacterial blight of sugar beet caused by *Pseudomonassyringae pv. aptata*) in sugar beet [86]. An image database was created with infected crop under controlled as well as field conditions with over 1870 images of diseased (1420 images) as well as healthy leaves (450 images). The data processing started with region detection, where the areas of interest were identified based on the shapes and RGB pixel values. Then, feature extraction was performed to compute the following values from the RGB values: (i) red-channel (R), (ii) green-channel (G), (iii) blue-channel (B), (iv) intensities (INT), (v) local binary patterns (LBPs) of intensities (INTLBP), (vi) gradient magnitudes (Gmag), (vii) gradient directions (Gdir), and (viii) LBPs of gradient magnitudes (GmagLBP). Next, a one-versus-one multi-class support vector machine (SVM)-based classifier with radial basis function (kernel) was trained using the extracted parameters. The accuracy of the sensing system was given by,

$$Accuracy = \frac{TN + TP}{FN + FP + TN + TP}, \quad (1)$$

where FN = false negative, FP = false positive, TP = true positive, and TN = true negative. The accuracy values between 68% (for *Phoma* leaf spot) and 90% (Beet rust) were reported.

A smartphone-based image processing application for plant disease diagnosis was reported in [88], where the developed system was tested for vineyard diseases based on photographs of grape leaves. The analysis begins by isolating region lesions (areas of interest or disease) from background (assumed to be significantly brighter than the leaf by using a white colored background while imaging) and healthy tissue through thresholding of the RGB pixel values. Then, the following lesion features are extracted: number of spots, their gray level and area, followed by a histogram construction indicating the number of pixels that have a specific red, green, or blue color level. For test images, the color histograms are extracted and compared within the predefined limits, and the top three possible diseases are indicated. Success rate of about 90% were observed.

An imaging system for continuous plant level (single leaf based) monitoring of *Cercospora* leaf spot (CLS) in sugar beet by template matching and pattern recognition was presented in [92]. The first stage employs a robust template matching strategy called orientation code matching (OCM) for continuously tracking a single leaf of a plant over

time by searching for its corresponding position based on the matching of orientation codes (OC) between two images from adjacent image frames. The second stage uses SVM with radial basis function kernel as pattern recognition method for classifying CLS against the field background using the following three features derived from RGB images as inputs: L^* , a^* , and entropy \times density, where entropy and density of an image represent richness of intensity and contrast, respectively. Although, high classification accuracy (above 95%) was achieved, in case of real-world application, precision values ($\frac{\text{true positive}}{\text{all positive}}$) between 30% to 83% were observed with better results in case of infection in older leaves than younger ones which was attributed to more saturated RGB colors (darker green and better contrast) in the older leaves.

A multi-plant multi-disease detection system using digital image processing was developed in [90], where disease identification was performed based on color transformations, color histograms and a pairwise-based classification system. Unconstrained set of leaf images were taken from 12 different plant species under 82 different stresses (74 biotic, 4 pests, and 4 abiotic) using common digital cameras and mobile devices with 15% in controlled laboratory conditions while 85% in the field. The first task in data processing was the leaf segmentation to remove the background, done using guided active contour (GAC) method. The second step was symptom segmentation, which is identifying the boundary between disease tissue and healthy tissue on a leaf. Four segmentation masks were generated as binary functions of the parameters, r_1 and r_2 , which can be defined for each pixel as follows:

$$r_1 = R/(G + e), \quad \text{and} \quad r_2 = B/(G + e), \quad (2)$$

where R , G , and B are the pixel values of the red, green, and blue channels of the RGB representation, respectively, and e is an arbitrarily small value for avoiding divisions by zero. Next, the segmented RGB images were transformed arithmetically to generate ten new color channels (H , S , V , L , a , b , C , M , Y , and K). A color-channel-based pairwise classification approach was applied to address the problem that many of the diseases present quite similar visual symptoms (classes not well defined), and one approach was to divide the problem containing c classes into $c(c - 1)/2$ binary (or two-class) problems. In the training process, a 100-bin reference histogram was generated for each disease and color channel aimed at capturing the general behavior of each disease for all color channels. The color channels, whose reference histograms correlated the least for each pair of diseases, were taken as the ones with the best discriminative capabilities for those pairs, and used in the next step. Next, the cross-correlations between each selected reference histogram and the histograms of all corresponding images in the training set were calculated and averaged, resulting in a consistency value (the closer it is to one, more consistent was the color channel for that disease). For the test images, the corresponding histograms were generated and cross-correlations with the reference histograms as well as the consistency values were calculated. Then, a maximum likelihood operation was performed to estimate the most likely disease. Accuracy of about 58% was observed while the correct disease was ranked in the top two or three likely diseases in about 80% of the cases.

An image-based multi-plant multi-disease detection system was reported in [89], where a public dataset (PlantVillage) of 54,036 images (of 14 crop species with 26 diseases) collected under controlled conditions of diseased and healthy plant leaves were used to train deep learning networks for classification. The applicability of deep convolutional neural networks (DCNN) with focus on AlexNet and GoogLeNet were evaluated for the classification problem. Both the DCNNs were computationally intensive during training phase but faster under testing. The reported system achieved a top accuracy of 99.35%. However, when tested on a set of images taken under conditions different from the images used for training, the model's accuracy reduced substantially, to just above 31%.

A monochrome vision-based system for detecting Huanglongbing (HLB) disease in citrus trees (particularly, orange) was developed in [93], where increased level of starch accumulation in HLB-symptomatic leaves was characterized using the rotation of the

polarization of light by 90° at 591 nm. The imaging set-up consisted of a monochrome camera equipped with a wide lens (6 mm focal length) and a rotating polarizer housed inside a wooden box with an light emitting diode (LED) diode panel for illumination at 591 nm. Sixty citrus leaf samples were acquired in laboratory setting while 30 in the field setting from four known classes: HLB-positive, HLB-negative, zinc deficient HLB-positive, and zinc deficient HLB-negative. qPCR was performed in order to verify the HLB status of all the samples. The gray scale histograms of the symptomatic areas were obtained for each image for classification, where gray value (ranging between 1 and 255) represented the light intensity for each pixel. The mean and standard deviation (SD) of the gray value were extracted from the normalized histograms, and were used to train a support vector machine (SVM)-based maximum margin classifier. A three-fold cross validation method was employed in the classification process in which the dataset was randomly divided into three folds, two were used for training and one for validation. This process was repeated fifty times, and the average classification accuracy of about 97% was achieved.

An automatic multi-disease diagnostic system for detecting three diseases in wheat, septoria, rust, and tan spot, using common mobile capture devices was reported in [87]. The image analysis was carried by first pre-processing the images by means of color constancy algorithms to minimize natural illumination variability effects. Next, leaf segmentation was performed, where automated as well as user assisted approaches were developed. Finally, during disease classification step, a primary segmentation was done in order to detect and select any suspicious sub-region on the leaf as a disease candidate (hot-spots). Each obtained hot-spot region was described by means of two visual descriptors: color and texture. For each disease and descriptor, a Random-Forest based classifier was trained providing a hot-spot-based disease feasibility value. Then, a meta-classifier module weighed all individual decisions to make a global assessment. The algorithm was deployed on a real smartphone application and validated under real field conditions in a pilot study located in Spain and Germany with over more than 36 wheat varieties, where an overall accuracy of 80% was achieved.

An image processing-based wireless sensor network (WSN) for vineyard monitoring was reported in [94], where each sensor node consisted of a webcam mounted on stepper motor (that can rotate to cover a wider field) connected with a wireless router for communication. The sensor nodes were scattered across the vineyard on 6 m high posts to get a clear field of view and avoid any obstruction in the line of sight for communication. The image processing began with thresholding, which uses the RGB data as well as the hue, saturation, value (HSV) data, derived from RBG images, to distinguish healthy (green) leaves from unhealthy (discolored) leaves. Second, the leaf size was estimated based on mean pixel variation in the parts of the image corresponding to the healthy (green) tissue. It was shown that green (or healthy) leaves appearing smaller in the image (due to being farther from the camera) show greater pixel variation, or normalized difference index (NDI) which was defined as:

$$NDI = \frac{G - R}{G + R}. \quad (3)$$

Next, a set of morphological operations using masks to smooth boundaries, fill holes, and remove artifacts were applied to reduce noise without eliminating useful features. Finally, in the detection step, the diseased leaves ratio in each image was calculated as the ratio of the features left in the mask (after previous operations) and the leaf size (to eliminate the effect of dead leaves on the ground), based on which the plant health was determined. Overall, a WSN-based sensing system at the field level was demonstrated but no performance metrics like accuracy were mentioned.

In general, RGB-imaging-based methods are particularly suitable for general plant health monitoring and in most cases, common imaging devices such as smartphones or digital cameras can be employed making the sensing set-up inexpensive. However, the classification of diseases is often computationally intensive while exhibiting moderate accuracy.

3.2.2. Hyperspectral Imaging

Hyperspectral (HS) imaging-based systems have emerged as a promising technology for fast non-contact/non-invasive sensing and has been successfully applied in the field of plant disease diagnostics. In contrast to RGB imaging, where the extracted information is based on color spaces, in HS imaging the reflected light from the plants is segregated into hundreds of narrow spectral bands across the EM spectrum to obtain a hypercube (images comprising of two spatial and one wavelength dimensions), which is then characterized using sophisticated data processing algorithms (see Figure 8). Unlike, visible/RGB imaging which only captures images from 400 nm to 700 nm wavelengths (visible region of the EM spectrum), hyperspectral imaging systems are designed to capture spectral as well as spatial information beyond the human vision ranging from ultraviolet (UV) to shortwave infrared (SW-IR) wavelengths, between 350 nm and 2500 nm. Different wavebands may offer diverse information, where healthy plants typically absorb visible light (VIS 400–700 nm) strongly due to chlorophyll/photosynthesis related pigments, whereas the light scattered in the near-infrared (NIR 700–1000 nm) is largely dependent on the leaf cell structure, and the leaf reflectance in the SW-IR (1000–2500 nm) is influenced by the leaf water and chemical content [95]. Therefore, HS images can offer rich spectral information leading to better characterization, modeling, classification, and detection of diseases in plants.

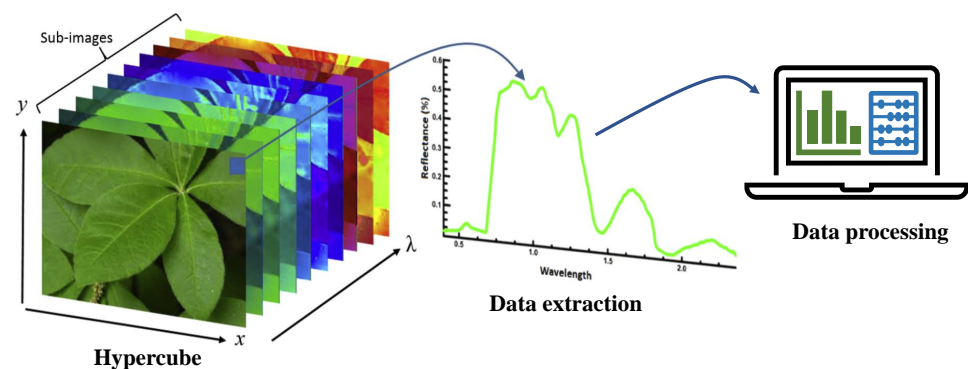


Figure 8. General workflow of hyperspectral imaging-based plant disease detection. Adapted from [96], Copyright (2017), with permission from Elsevier.

In addition to specialized HS imaging camera set-up, data processing software is also crucial. Various image processing strategies in the HS domain have been applied for predictive crop disease modeling, including empirical models, and machine learning-based algorithms. Several works on HS analysis for plant disease detection have been reported in literature of which some of the key recent works are discussed here, and a brief comparison is presented in Table 4.

Table 4. A comparison of the key recent hyperspectral (HS) imaging-based sensing methods for monitoring pathogenic stress in plants.

Sensing Application	Brief Description	Accuracy	Strengths	Limitations	Ref., Year
Target spot and bacterial spot in tomato	35 spectral vegetative indices and 2 classifiers were evaluated using UAV-based and benchtop-based HS imaging.	97% to 99%	Good accuracy, in-field as well as laboratory-based operations were developed and compared	Computationally intensive, spatial resolution as well as specificity not discussed	[97], 2020
Early TSWV detection in sweet pepper	Analysis method based on generative adversarial nets, named as outlier removal auxiliary classifier generative adversarial nets (OR-AC-GAN) was presented	96.25%, under controlled conditions	Early disease detection capability exhibited, all-in-one method (from image segmentation to classification)	Computationally complex, special hardware required, in-field testing not explored	[98], 2019
Charcoal rot in soybean	RGB-imaging-based segmentation followed by 3D CNN based classification	95.73%, under controlled conditions	Importance of specific hyperspectral bands using saliency map visualizations was studied	Not applicable for early detection, in-field operation not explored	[99], 2019
Yellow rust in winter wheat	Drone-borne HS imaging system, where vegetative index value was used to identify vegetation, and a DCNN-based model was employed for classification	85%	Field-deployable, good accuracy and resolution	Expensive hardware, complex computations required	[100], 2019
Early detection Of TMV in tobacco plant	Spectral as well as textural features were extracted, where several machine learning algorithms were evaluated to classify disease stages with effective wavelengths, texture features, and data fusion, respectively	95%	Good accuracy, early disease detection exhibited	Computationally complex, no clear conclusions were made on selecting a machine learning classifier	[101], 2017
TSWV detection in capsicum plants	Discriminatory features were extracted using the full spectrum, a variety of vegetation indices, and probabilistic topic models. An SVM-based classifier was trained	90%	Good accuracy under controlled imaging conditions	Requires sophisticated hardware and complex software, in-field operation not evaluated	[95], 2017
Late blight and early blight in potato	10 different spectral and textural features were extracted and a multi-class SVM-based classification model was developed	95%	Good accuracy under controlled imaging conditions	Dependent on visual features therefore, pre-symptomatic detection is not feasible	[102], 2017

TMV = Tobacco mosaic virus.

An HS reflectance imaging-based early detection system for tomato spotted wilt virus (TSWV) in tomato plants was reported in [98], where a machine learning based sensing platform named outlier removal auxiliary classifier generative adversarial nets (OR-AC-GAN) was developed. OR-AC-GAN is a variant of generative adversarial network (GAN), a neural network architecture in deep learning domain [103]. The developed method integrates the tasks of plant segmentation, spectrum classification and image classification. The OR-AC-GAN model used 83 wavebands between 395 nm and 1005 nm and was shown to achieve an average classification accuracy of 96.25% before the appearance of visible symptoms, as early as 5 days after inoculation (DAI). Additionally, the combination of OR-AC-GAN with three band selection algorithms was explored, where maximum variance principle component analysis (MVPCA)-based band selection technique provided similar accuracy as stand-alone OR-AC-GAN but with 8 spectrum bands.

In addition to the spectral features like, reflectance or transmittance at different wavelengths, HS images also contain images-based spatial features like, textural properties. Traditionally, only spectral features are extracted from the HS images, however texture-based variables may additionally provide supplementary information leading to better accuracy in classification. An early rapid tobacco mosaic virus (TMV) infection detection system using HS imaging in the VIS/NIR spectral region (380 nm to 1023 nm) was reported in [101], where both spectral and textural features at selected wavelengths were used for four-class classification (healthy, 2 DAI, 4 DAI, and 6 DAI). Coupled with the successive projections algorithm (SPA) and machine-learning-based classifiers, correlations were established among the reflectance spectra, texture features, and the stage of diseased development. Based on SPA, 8 out of 434 EWs were selected, where majority of the EWs were found to be in the short-near infrared region. A broad set of classifiers were evaluated, including partial least squares-discrimination analysis (PLS-DA), random forest (RF), support vector machine (SVM), back propagation neural network (BPNN), extreme learning machine (ELM), and least squares support vector machine (LS-SVM). The classification was performed for three different datasets at the selected EWs: spectral features, textural features (contrast, correlation, entropy, and homogeneity), and data fusion (both spectral and textural features). ELM classifier resulted in the best overall classification accuracy of 98.33% using only spectral features, whereas a maximum accuracy of 93.33% was achieved using BPNN classifier with textural variables, and around 95% accuracy was achieved with data fusion using BPNN classifier.

A sensing system for TSWV disease detection in capsicum plants using HS imaging was developed in [95], where SVM classifiers on three types of features: the full spectrum, spectral vegetative indices (VIs), and features generated using data driven probabilistic topic models, were trained on both VIS-NIR and SW-NIR hypercubes resulting in over 90% accuracy. The HS imaging system consisted of two push-broom hyperspectral cameras from Headwall, the VNIR A-series, and the SWIR M-series, and six 20 W halogen lights for illuminating the leaf sample. A thread grid was used to hold the leaf sample flat against the plate during imaging, and for reference, the image with camera cap “on” served as the 0% reflectance, while the image of a standard white teflon target served as the white reference (99.9% reflectance). Prior to classification, hypercube pre-processing was performed to segment the leaf from the background in the spectral domain (by an unsupervised K-means clustering algorithm), and grid removal (by spatial matched filter approach).

In another work, an HS imaging-based system for early detection of *Phytophthora infestans* (late blight) and *Alternaria solani* (early blight) diseases in potato was presented in [102], where SVM-based supervised learning model was developed using spectral, textural, and contextual features. A total of 300 images of potato leaves spread across the three class labels, late blight affected, early blight affected, and healthy leaves, were analyzed. The images were taken from a publicly available database, plant village (www.plantvillage.com). Firstly, leaf segmentation was performed using the mask filtering process to identify and select the regions of interest. Next, 10 different features/variables were selected for SVM

(multiclass with linear kernel)-based classification. Of the 300 images, 180 were used for training and 120 for testing, where 95% classification accuracy was achieved.

A deep convolutional neural network (DCNN)-based approach for automated yellow rust disease (caused by *Puccinia striiformis f. sp. Tritici*) detection in winter wheat using a unmanned aerial vehicle (UAV) based HS imaging system was reported in [100], where the study was conducted over a whole crop cycle on four 220 m² plots, two infected with the disease and two healthy. HS imaging was conducted five times using a UHD 185 firefly sensor (Cubert GmbH, Ulm, Baden-Württemberg, Germany) mounted on a DJI S1000 UAV system, where reflected radiation between 450 nm and 950 nm with a total of 125 bands was captured from a height of 30 m (resolution of 2 cm per pixel). Normalized difference vegetation index (NDVI) was calculated and used to separate vegetation from bare soil in the images, where NDVI greater than 0.3 was labeled as vegetation. In the data pre-processing step, sliding window image segmentation algorithm was implemented to extract spatial and spectral information. Next, a DCNN model comprising of multiple Inception-Resnet blocks was used for feature extraction followed by an average pooling layer and a fully connected layer for transforming the feature maps into a three-class classifier: rust, healthy, and other. An accuracy of 85% was observed at the field scale.

In another work, a 3D-CNN-based model for the detection of charcoal rot disease (caused by the fungus, *Macrophomina phaseolina*) in soybean was reported, where the data pre-processing consisted of using RGB wavebands of the HS images for the segmentation of the charcoal rot stem [99]. The RGB images were transformed to HSV color space, followed by segmenting of the charcoal rot stem by simple thresholding. Healthy and infected soybean stem samples were collected at 3, 6, 9, 12, and 15 DAI, and 3D-CNN model was used to extract features jointly across the spatial and spectral dimension for classification. The 3D-CNN model consisted of two convolutional layers interspersed with two max pooling layers followed by two fully connected layers, and was able to achieve a classification accuracy of 95.73% across 539 test images. Additionally, saliency map visualizations of the healthy and infected samples were constructed to study and explain the importance of specific hyperspectral wavelengths in classification.

In a comparative study, a UAV-based and a benchtop-based HS imaging (380 nm to 1020 nm) system for detecting target spot (caused by fungus *Corynespora cassicola*) and bacterial spot (caused by *Xanthomonas perforans*) diseases in tomato were developed and compared [97]. Tomato leaves were classified into four categories: healthy, asymptomatic, early, and late disease development stages, while 35 spectral vegetation indices (VIs) were calculated and evaluated for optimal detection response. Two different classification methods were utilized: (i) multi-layer perceptron neural network (MLP) and (ii) stepwise discriminant analysis (STDA), and compared. Based on the analysis, it was reported that the most significant VIs include photochemical reflectance index (PRI) for both diseases, the normalized difference vegetation index (NDVI850) for bacterial spot in all stages, and the triangular vegetation index (TVI), NDVI850, and chlorophyll index green (Chl green) for target spot (TS) asymptomatic, TS early, and TS late disease stage, respectively. Of the classification methods, MLP-based classifier exhibited superior classification accuracy of 99% under field (UAV-based) and laboratory conditions.

In addition to the aforementioned works, several other HS imaging-based crop disease detection systems have been reported in the past decade or so [104,105]. In general, HS imaging is active area of research for *pre-symptomatic crop health monitoring*. Though computationally intensive, reasonably selecting spectrum wavebands, and analysis methods can reduce the computation time for sufficient accuracy, providing potential for automated in-field applications. However, unlike RGB-imaging, specialized hardware (HS cameras) is required which make the method expensive.

3.2.3. Thermography

According to Planck's radiation law, every object at temperature above absolute zero emits electromagnetic radiation (blackbody radiation), and the amount of radiation emitted is a function of its emissivity (ϵ) and absolute temperature (T), and can be given according to the Stefan–Boltzmann law as,

$$W = \epsilon\sigma T^4, \quad (4)$$

where W is the spectral radiant emittance (in W/m^2), and σ is the Stefan boltzmann constant ($=5.67 \times 10^{-8} W m^{-2}K^{-4}$). Thermography is a non-contact method for plant health monitoring, where surface temperatures of leaves, plants, or crop canopies are observed using their inherent thermal radiation. The emitted infrared (IR) radiation is recorded using thermographic cameras in the IR wavelength region of 8–12 μm to produce false color images, where each pixel relates to a particular temperature value. The principle of detection is based on the disturbances in stomatal conductance, photosynthesis, and transpiration in a diseased plant, leading to thermal variations in the plant tissue that may act as indicators of stress [106].

An application of thermal imaging for rapid diagnosis of crop disease was reported in a recent study, where tomato mosaic disease and wheat leaf rust were taken as examples [107]. Leaf temperatures were continuously monitored for the two crops during the incubation period. The results showed that the maximum temperature difference (MTD) of the tomato mosaic disease ranged from 0.2 °C~1.7 °C, and that of wheat leaf rust ranged from 0.4 °C~2 °C. As the disease progressed, the MTD of both plants showed an increasing trend while the average temperature decreased. The variations in MTD were evident 5 to 7 days prior to the visible symptoms, demonstrating the early disease detection capability of thermography.

In another work, the suitability of IR thermography was assessed for sensing scab disease in apple caused by the phytopathogenic fungi, *Venturia inaequalia*, colonizing apple leaves below the cuticle [108]. It was observed that the fungal growth caused localized decrease in temperature before symptoms appeared that significantly increased the MTD of leaves. The MTD increased linearly with the size of the infection ($R^2 = 0.85$), and later decreased due to leaf senescence.

A UAV-borne thermal system for detecting disease-induced canopy temperature increase due to red band needle blight (caused by the fungus *Dothistroma septosporum*) in pine plantations was presented in [109]. Sixty sample trees were surveyed and thermal imagery was acquired at six different times of a day from an altitude of 60 m. Statistically significant correlation between canopy temperature depression (CTD) and disease levels was observed with R^2 between 0.27 and 0.41, which may be related to the needle damage symptoms caused by the disease, i.e., loss of cellular integrity, necrosis, and eventual desiccation. Additionally, the inclusion of light detection and ranging (LiDAR)-based structural metrics (changes in canopy structure with disease) in the overall disease detection analysis was studied, and only a slight improvement was observed.

A pre-symptomatic detection mechanism for cucumber downy mildew (caused by oomycete, *Pseudoperonospora cubensis*) using thermography and fourier transform infrared (FTIR) spectroscopy was reported in [110]. First, using thermal imaging under controlled conditions, it was observed that MTD-based detection was possible at 4.42 DAI, whereas visible symptoms appeared after 5.36 DAI. However, MTD peaked at around 7 DAI after which it decreased sharply. Second, the FTIR spectra was obtained from the regions between the diseased and healthy areas at three characteristic wavenumbers: 2977 cm^{-1} , 1544 cm^{-1} and 1050 cm^{-1} for pre-symptomatic analysis. At these points, maximum variation between the spectra for healthy and disease regions occurred, which was used to distinguish between the pre-symptomatic, visually detectable, and later stages of downy mildew disease progression in cucumber leaves.

Several other works have been reported regarding the use of thermography for disease detection in plants including (i) a thermal vision system for identifying powdery-mildew and gray-mold disease in rose plants [111], where the regions of the interest in thermal images were identified by segmenting the corresponding visual images. Performance of the designed neuro-fuzzy classifiers were evaluated with the thermal images captured using an automatic imaging setup and correct estimation rates of 69% and 80% were achieved at 2 DAI; (ii) thermographic visualization of leaf response in cucumber plants infected with the soil-borne pathogen *Fusarium oxysporum f. sp. cucumerinum* (FOC) [112], where the variations in the MTD, transpiration rate, stomatal conductance, and relative membrane injury were studied. Correlations between FOC infection stages and the mentioned parameters were observed.

Overall, thermography-based sensing methods are relatively less computational as compared to RGB or HS imaging methods, but require special camera equipment and can only provide generalized indication of biotic stress in plants, exhibiting poor specificity.

3.2.4. Non-Imaging Spectroscopic Methods

Non-imaging spectroscopic methods include Visible/Infrared (VIS/IR) reflectance and transmittance spectroscopy-based methods, and Raman spectroscopy-based approaches. The VIS/IR spectroscopy is a subset of hyperspectral imaging where only the spectral information (and not spatial/pixel information) in the VIS/IR wavelength region is recorded. Either the reflectance of the leaf/tissue surface or the transmitted light through the leaf tissue is measured and correlated with the plant health. A VIS-NIR reflectance spectroscopy-based system for detecting HLB or citrus greening disease in citrus trees was reported in [113], where two portable halogen lamps (as light source) and a field-portable SVC HR-1024 spectroradiometer (Spectra Vista Cooperation, NY) were used to collect the reflectance data between 350 nm to 2500 nm (989 data points). The complete system also consisted of a laser pointer to denote the area for which the data were recorded, and was mounted on a mobile platform for in-field operation. Various classification algorithms were tested where quadratic discriminant analysis (QDA)-based algorithm yielded the highest overall average classification accuracy of about 95%. In another work, NIR spectroscopy was evaluated as a method for detecting zebra chip (ZC) disease (caused by *Candidatus Liberibacter solanacearum* bacteria) in potatoes [114]. A bench-top spectroradiometer was used for obtaining spectral information for each individual potato where two models were tested: (i) direct correlation between spectra and ZC, and (ii) correlating sugar content in potatoes with ZC. Stepwise regression in conjunction with canonical discriminant analysis (CDA) was applied to the raw spectra where a total classification accuracy of 98.35% was achieved. The same analysis when applied to second derivative spectra yielded 97.25% accuracy. Alternately, CDA applied to sucrose, glucose, and fructose concentrations previously determined by HPLC yielded 96.7% classification accuracy.

Several other recent works have been reported on spectroscopic methods for plant disease detection including (i) investigation of early detection of potato late blight using contact leaf reflectance measurements with a spectroradiometer where the leaf was clipped on to a surface and illuminated with halogen light sources [115]. The spectral responses were measured for two different genotypes (one with a resistance gene) and at different stages of infection: early infection, biotrophy, necrotrophy, and sporulation. Three different classification approaches: random forest discrimination (RF), partial least squares discrimination analysis (PLS-DA), and normalized difference spectral index (NDSI) were applied where accuracy between 60% to 85% were obtained for each technique; (ii) detection of pepper fusarium disease under laboratory settings using spectral reflectance and a K-nearest neighbor (KNN)-based classifier where a classification accuracy of over 90% was achieved, however specificity with respect to other diseases was not evaluated [116]; (iii) NIR spectroscopy-based detection of bitter pit disorder in honeycrisp apples where the spectra for 40 apples (20 healthy and 20 bitter pitted, kept in cold storage) were recorded at 0, 35, and 63 days after harvest [117]. Spectral data in the nine spectral bands (though to be

associated with bitter pit) between 971 nm and 1143 nm were collected and classified using QDA and SVM-based classifiers yielding an average accuracy in the range of 78% to 87%.

Overall, non-imaging VIS/IR spectroscopy (VIS/IR-spec) exhibits some unique strengths like simpler experimental set-up consisting largely of a light source or lamp and a spectroradiometer making it relatively cheaper as compared to HS imaging. Moreover, data analysis procedures are relatively non-complex as image pre-processing steps are no longer needed. However, unlike HS imaging, VIS/IR-spec lacks spatial information making it difficult to implement under field settings (special data capturing apparatus is required) as there can be significant interference from the surroundings. Additionally, imaging-based techniques can capture textural features providing functional supplementary information leading to greater scope for pre-symptomatic crop disease detection with relatively higher specificity.

Raman spectroscopy (RS) is the other analytical spectroscopic technique that provides information related to the molecular structure of the specimen based on the molecular vibrations through inelastic photon collisions (by shining a laser beam at the object). Figure 9 shows the schematic of a general Raman-spectroscopy-based plant health monitoring system. In a recent work, the detection and identification of fungal pathogens (*spergillus flavus*, *A. niger*, *Fusarium* spp., or *Diplodia* spp.) in maize kernels using a hand-held Raman spectrometer was explored [118]. The Raman spectra from individual maize kernels was recorded using a hand-held portable Rigaku Progeny ResQ spectrometer (Rigaku Analytical Devices, Inc., Wilmington, MA, USA), equipped with a 1064 nm Nd:YAG laser. Next, multivariate data modeling based on orthogonal partial least-squares discriminant analysis (OPLS-DA) was performed where in the final step, 4 predictive components, 3 orthogonal components, and 391 out of 512 original wavenumbers, were used to generate the misclassification table. It was demonstrated that the model was able to classify the four disease with 100% accuracy. However, the method was applied for post-symptomatic (tissue already damaged) analysis where the information about the extent of infection (sampling at a particular DAI) was missing as well as the number of sample were not clearly disclosed. Moreover, the kernels were extracted from the cob and placed in special apparatus before analysis making the sampling process complex.

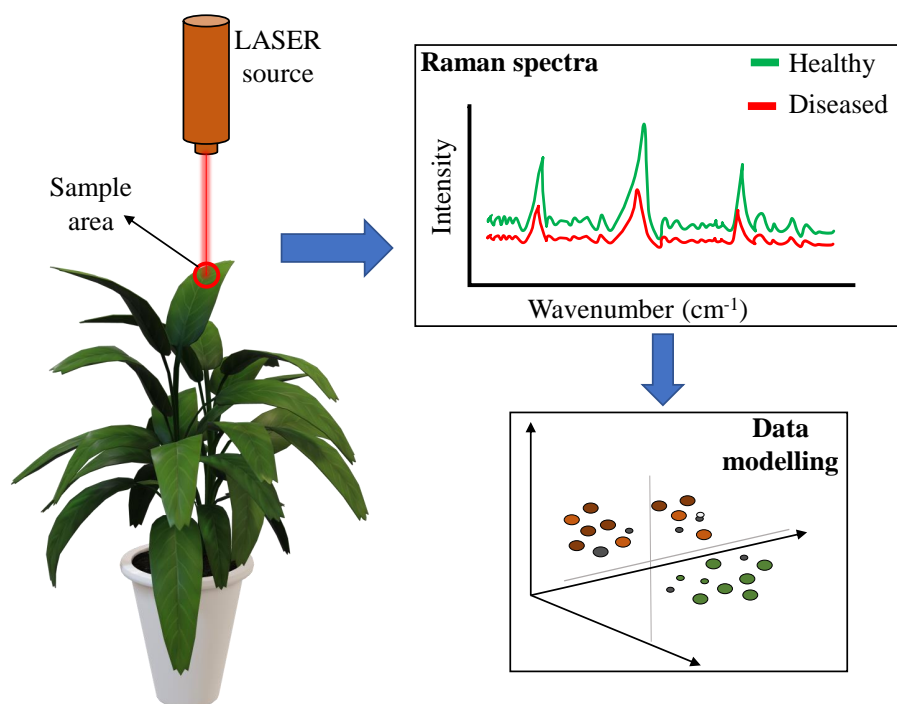


Figure 9. Schematic of Raman spectroscopy-based plant health monitoring system.

Other recent works on RS-based plant disease detection include (i) A handheld RS-based system for the detection of *Abutilon mosaic virus* (AbMV) in *Abutilon* (ornamental crop) was reported in [119] where spectra of leaves from healthy and infected plants were recorded, and difference in the intensity of the bands, particularly the one at 1526 cm^{-1} , was proposed as a basis for the early detection. An accuracy of 99% was reported with a coherent intensity variation across all bands which indicates the lack of specificity, and may occur due to general discoloration of the infected leaf; (ii) diagnosing of citrus greening (or HLB disease) from the Raman spectra of citrus leaves, obtained using a SENTERRA confocal microprobe Raman spectrometer [120]. The samples were divided in to five infection categories: serious, moderate, slight, nutrient deficient, and healthy. Identification of spectral peaks of interest and background removal was done by taking first derivative and linear fitting while the spectral variables were screened using PCA- and SPA-based methods in the range 715.0 to 1639.5 cm^{-1} . Next, PLS-DA was applied for classification and a recognition rate of 100%; (iii) early detection and discrimination of two economically important viral infections (caused by tomato yellow leaf curl Sardinia virus; TYLCSV and TSWV) in tomato plants [121], where manually inoculated plants were monitored over 28 days with samples tested using RS and PCR. PCA and PLS-DA-based analyses were performed for feature selection and classification, respectively yielding accuracy of over 70% for TYLCSV at 14 DAI and over 85% for TSWV at 8 DAI. The scope for using RS-based method for early detection of common viral diseases in tomatoes was demonstrated.

In general, RS-based methods hold greater potential than VIS/IR-spec for specific disease identification, and a growing number of RS-based studies are being reported with high accuracy plant disease detection where hand-held portable systems have been demonstrated. However, some drawbacks associated with the technique include relatively higher cost of equipment, complex data analysis, and susceptibility to background fluorescence from chemical as well as physical (for example, dirt) compounds. Furthermore, the sample area of a typical Raman spectrometer probe (laser beam) is of the order of 10s of microns which if not focused appropriately may lead misdiagnosis as the infection in the plant tissue may not spread uniformly, and the high energy beams may lead to undesired tissue damage.

3.2.5. Chlorophyll Fluorescence Imaging

Chlorophyll fluorescence (ChlF) imaging is a relatively new method applied towards disease detection in plants. Light energy absorbed by chlorophyll molecules in the leaf can (i) drive photosynthesis (photochemistry); (ii) be re-emitted as heat; or (iii) be re-emitted as light (fluorescence). All the three processes compete with each other and can provide information about quantum efficiency and heat dissipation, and indirectly the plant health. ChlF is particularly a measure of the re-emitted light in the red part of the EM spectrum from Photosystem II (water-plastoquinone oxidoreductase; PS-II)-based photo-chemical reaction [122]. The ChlF-based sensing principle involves illuminating a darkness adapted plant and recording the fluorescence spectra, which is dependent on the photosynthetic apparatus of the leaf that in turn is dependent on the plant's health. In general, a depression in the ChlF value is observed as pre-symptomatic indication of plant disease.

Several works have been reported on ChlF-based imaging including (i) a thermography versus ChlF imaging for detection and quantification of apple scab [123], where it was reported that thermography exhibited higher sensitivity; (ii) the detection of sweet potato feathery mottle virus (SPFMV) and sweet potato chlorotic stunt virus (SPCSV) in sweet potato using thermal imaging and ChlF [124], where it was demonstrated that the operating efficiency of PS-II and photochemical quenching were the most sensitive parameters for the quantification of virus effects compared with maximum quantum efficiency, non-photochemical quenching, and leaf temperature; (iii) an early detection system using HS- and ChlF-imaging in conjunction [125]. Combining both techniques in one device that also guaranteed integrated and congruent images reduced classification errors to less than 5%.

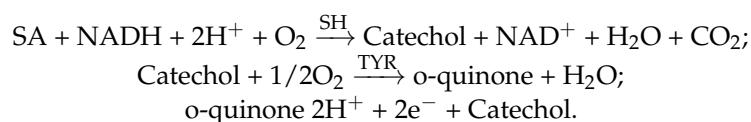
Overall, the ChlF imaging is mainly applied towards phenotyping applications and provides insight into the photosynthetic processes in plants, and is largely applied to plant disease detection in conjunction with other imaging methods to improve accuracy [125,126]. However, because of the need for dark adaptation before imaging, the method has limited potential for fast in-field crop health monitoring.

3.2.6. Biosensing Methods for Phytohormones Detection

As mentioned previously in Section 2.1, the onset of SAR is one of the key ways plants achieve immunity and the phytohormones SA, JA, and ET play critical roles in the signaling process. Therefore, sensing the levels of these hormones have been used as indicators of stress in plants. Conventionally, the phytohormones are detected under laboratory conditions using standard analytical techniques like high-performance liquid chromatography-mass spectrometry (HPLC-MS) [127–129]. In general, these methods require extensive sample preparation involving analyte-specific extraction chemistry followed by ionization, separation, and quantification of the ions on the basis of their mass/charge ratio. Alternative to analytical methods (which are time, cost, and labor intensive while being largely restricted to laboratories), several biosensing methodologies for fast, portable, and economical detection phytohormones have been developed, including enzymatic sensors, aptamer-based sensors, molecularly imprinted polymer (MIP)-based sensors, and electro-catalysis-based sensors. Key recent advances in detecting primary defense-related hormones, SA, and JA are presented here, while sensing methods for ET/VOCs are described later in Section 5, as they largely correspond to both pathogenic and pest-based stresses in the plants.

SA Detection

An enzymatic sensing approach for the detection of methyl-salicylate was reported in [130], where a bi-enzyme recipe containing the enzymes, Salicylate hydroxylase (SH) and Tyrosinase (TYR) was employed. The sensors was fabricated on a glassy carbon (GC) electrode exhibiting a sensitivity of about $30.6 \mu\text{A cm}^{-2} \mu\text{M}^{-1}$. The principle of detection was based on the bi-enzyme-based reactions as follows [131]:



In another work, a bi-enzyme microfluidic electrochemical sensor utilizing the enzymes SH and TYR recipe on graphene oxide substrate was reported [24]. The sensing device consisted of 3-electrode system forming a 3D structure and was characterized using chrono-amperometry while showing a sensitivity of $34.4 \mu\text{A cm}^{-2}$ per decade change in SA concentration in (μM).

A structure-switching aptamer-based sensor for SA determination was reported in [132], where the identified SA aptamer was incorporated onto a nano-structured Fabry–Perot interference sensor, and the interference fringes of the reflected white light from the sensor were used as transducing signals for SA quantification. The sensor exhibited a detection limit of $0.1 \mu\text{M}$ with a range of $10^{-1} \mu\text{M}$ to $100 \mu\text{M}$, and the sensor was tested for SA determination in rice or *Arabidopsis* leaf samples. Aptamers are oligonucleotide or peptide molecules with affinity towards a specific target molecule often accompanied by structural changes during binding. The aptamer for SA-binding was developed as follows: the ssDNA library was hybridized to a short piece of capture complementary DNA (cDNA) immobilized on magnetic beads, where SA-binding induced conformational changes and subsequent de-hybridization from the captured cDNA, while the non-binders remained on the magnetic beads and could be removed. The SA binding sequences were further amplified through asymmetric PCR. In general, aptamers offer advantages like reproducible operation, low cost production, and tolerance to a wide range of pH and temperature changes as compared to other bio-agents like enzymes and antibodies.

A photo-electrochemical (PEC) sensor for SA detection using dual functional MIP-modified organometal lead halide perovskite ($\text{CH}_3\text{NH}_3\text{PbI}_3$), deposited on indium tin oxide (ITO) glass electrode, was presented in [133]. The MIPs precursors were prepared by thermally initiated free radical polymerization with SA as the template molecule, methacrylic acid (MAA) as the monomers, ethylene glycol dimethacrylate (EGDMA) as the cross-linker, and azobisisobutyronitrile (AIBN) as the initiator. Next, during film deposition of perovskite on the ITO glass, the MIPs precursor solution was added forming MIPs/ $\text{CH}_3\text{NH}_3\text{PbI}_3$ /ITO electrode, which was characterized by recording the photocurrent under illumination at different concentrations of SA. The developed sensor exhibited a linear relationship between the photocurrent changes and the logarithm of SA concentration from 7×10^{-13} M to 1×10^{-8} M with a detection limit of 2×10^{-13} M. Overall, the sensor displayed good selectivity and sensitivity but had limited range of operation.

In addition to aforementioned approaches employing bio-agents such as enzymes, aptamers, and MIPs, electro-catalysis-based sensors for SA detection have also been reported [25,134,135]. The working principle involves the characterization of the electro-oxidation of SA on metallic or carbon electrodes using electrochemical (EC) methods such as cyclic voltammetry (CV) and differential pulse voltammetry (DPV). The reaction mechanism of SA oxidation involves the formation of dihydroxybenzoic acids as the main product, and SA-polymeric compounds as additional products [134,135]. A low-cost bio-agent-free EC sensor for SA detection using electro-reduced graphene-oxide screen printed electrode was reported in [25], where the developed electro-oxidation-based device exhibited a range of 2 μM to 512 μM , with maximum sensitivity of 600 $\mu\text{A}/\text{mM}/\text{cm}^2$. The determination of SA through EC-oxidation on carbon-fiber electrode was presented in [135], where the developed sensor exhibited a linear range of 2 μM to 3 mM, with a limit of detection of 1.7 μM . A carbon tape electrode modified with handed pencil trace for real-time SA detection in infected tomato leaves was presented in [136], where a linear range of 10^{-6} M to 10^{-4} M, with a detection limit of 10^{-7} M was observed. Additionally, a selectivity test was performed with other common compounds that may be present in the plant sap such as indole-3-acetic acid, succinic acid, methyl jasmonate, abscisic acid, malic acid, and citric acid, where good selectivity was observed. In another work, a paper-based electroanalytical device for *in-situ* determination of SA in living tomato leaves was developed [137]. The sensor consisted of MWCNTs/nafion modified carbon tape electrodes, where a piece of the tomato leaf (with a small hole punched in) was sandwiched between the fabricated electrode and filter paper. The developed sensor exhibited a linear detection range of 0.5 to 100 μM .

JA Detection

Relatively fewer sensing systems have been reported for JA detection (when compared to SA sensing) where most of the research has been limited to JA determination in laboratory-based settings using analytical methods. An analytical method for the determination of JA in plant tissue using HPLC with fluorescence detection (HPLC-FD) was reported in [138]. Soybean mosaic virus-infected leaves were collected and the samples were prepared by grounding the frozen leaves (in the presence of liquid nitrogen) in to a powder, followed by addition of acetonitrile and ultrasonication at 4 °C, and finally, the extractant was obtained through centrifugation. Next, the derivatization (or labeling) of JA was performed in the presence of 1,3,5,7-tetramethyl-8-aminozide-difluoroboradiaza-s-indacene (BODIPY-aminozide), which exhibits strong fluorescence. Using BODIPY-aminozide as a precolumn derivatizing reagent, HPLC-FD was carried out yielding a range of operation of 5×10^{-10} M to 5×10^{-7} M, and a detection limit of 1.14×10^{-10} M. In another work, a methyl jasmonate (MeJA) EC sensor based on the electro-catalytic oxidation of the alkylene group in MeJA molecule using a phosphotungstic acid/graphene oxide (PTA/GO) nanohybrid modified graphite electrode was reported [139]. The sensor exhibited a detection range of 5×10^{-7} M to 8×10^{-5} M with a detection limit of 2×10^{-7} M in an acidic supporting electrolyte medium (0.1 M HClO_4).

Overall, phytohormone level-based plant health monitoring sensors hold great promise for conclusive (as compared to imaging-based or spectroscopic methods) stress detection. Understanding the role of SA and other hormones in various aspects of plant growth, development and interaction with its environment is a rapidly progressing area of research. Low-cost phytohormone sensing devices may provide a convenient way for pre-symptomatic disease detection and identification. However, in the present state, there is a need for developing not only innovative sensing technologies but also definitive correlations for hormonal activity and stress in plants.

4. Methodologies for Monitoring Herbivorous Pests/Insects

Herbivorous insect/pest detection methodologies can be classified into three broad categories: (i) imaging-based techniques, (ii) VOC monitoring-based detection, and (iii) acoustic methods for pest detection.

4.1. Imaging-Based Methods for Pest Detection

Similar to phytopathogen detection, several imaging-based methods have been applied towards plant pest detection, and key recent studies are discussed here. Table 5 presents a comparison of the key recent imaging-based sensing methods for herbivorous pest monitoring in crops. The general working principle is similar to RGB imaging-based phytopathogen detection, where the collected insect/pest images are processed to determine and segment the regions of interest, followed by the identification and classification of the insect/pest-based on the physical characteristics.

Table 5. A comparison of the key recent imaging-based sensing methods for herbivorous pest monitoring in crops.

Sensing Application	Brief Description	Perfor- mance	Strengths	Limitations	Ref., Year
Green- house insect pest monitoring	Sticky traps were used to sample pests for spatio-temporal monitoring, RGB images were classified using an SVM-based approach	93% (accuracy)	Good accuracy, low-cost system, and integrated humidity, temperature and light sensors	Lacks specificity	[140], 2020
Monitoring asian citrus psyllid in orchards	Ground-based vehicle was equipped with trapping and imaging set-up. Taken images were classified using CNN-based approach	80% (precision) 95% (recall)	Field-deployable, easy sampling of each tree, good performance	Expensive, not for generalized use (application specific)	[141], 2019
Monitoring banana corm weevil in banana	Various parts of the plants (shoot, fruit and leaves) were imaged, and three CNN-based architectures were evaluated	90% (average accuracy)	Large dataset created, good accuracy	Complex sampling procedure	[142], 2019
Multi-class pest detection (16 species)	Region Proposal Network (RPN) for providing pest regions and Position-Sensitive Score Map (PSSM) for pest classification and bounding box regression was proposed	75.46% (mAP)	Multi-pest detection system, created a large dataset, images were collected in-field conditions	Moderate accuracy, not fully automated	[143], 2019
Multi-class pest detection (10 pests)	A human-vision-inspired feature extraction model coupled with an SVM-based classifier was developed	85.5% (recognition rate)	Good performance, multi-pest sensing system	In-field operation was not demonstrated	[144], 2018
Detection of Thrips in strawberry greenhouse	A mobile robot equipped with photography hardware and software, image processing coupled with SVM-based classifier	2.25% (mean percent error)	Mobile system that travel along the rows of plants, good accuracy	Limited operation capability	[145], 2017
Monitoring Codling moths	Moths images were sampled in the field using pheromone traps. The images were then pre-processed, and classified using a CNN-based algorithm	93.4% (P-R-AUC)	In-field operation demonstrated, good performance	Specificity not tested, not automated	[146], 2016
Whitefly and Thrips detection in greenhouses	Sticky insect traps were imaged, the captured images were processed, and then, classified using a feed-forward multi-layer artificial neural network	92% to 96% (precision) using sample images	Semi-automated, good specificity between the insect species	Performance drops during in-field operation	[147], 2016
Detection of aphids in wheat fields	A maximally stable extremal region descriptor was used to process the images, and an SVM-based classifier was used for identification	86.81% (average accuracy)	In-field operation tested, moderate accuracy	Manual image collection procedure	[148], 2016

mAP = mean average precision; P-R-AUC = area under the precision–recall curve.

An automated vision-based system for monitoring Asian citrus psyllid (ACP) in citrus orchards using artificial intelligence (AI) was reported in [141]. ACP is a key pest of citrus due to its role as a vector of HLB disease. The system comprised of a modified ground-based vehicle equipped with the following: (i) a tapping mechanism to strike tree branches so that ACP may fall on a white board (serving as the sampling space), (ii) a grid of cameras to acquire images of the white board, (iii) a real-time kinematic Global Positioning System (RTK-GPS) to geolocate ACP detection, and (iv) NVIDIA Jetson TX2 embedded computational unit (NVIDIA TX2 Developer Kit, Santa Clara, CA, USA) for image processing. A two-step CNN-based ACP detection system was developed, where the first CNN was trained using You Only Look Once (YOLOv3), an object detection system [149] sensitive to ACP detection (all possible objects that can be ACP), but not accurate. The second CNN, based on YOLOv1, used the images from the first network's output for final classification. The developed system was used to test 90 trees in a citrus grove and displayed a precision ($\frac{\text{true positives}}{\text{true positives} + \text{false positives}}$) of 80% and recall of ($\frac{\text{true positives}}{\text{true positives} + \text{false negatives}}$) of 95%. The estimated cost of the automated vision-based ACP detection system was estimated to be around \$1000.

An automatic detection pipeline for identifying and counting pests in images taken inside field traps, using deep learning was proposed in [146], where Codling moths [150] were identified. Moths captured by pheromone traps containing an adhesive liner were imaged using a digital camera. The data analysis involved pre-processing using *gray-world* method to minimize variations due to imaging conditions and provide white-balanced images prior to detection. Then, a sliding window approach based on CNN was used, where a trained classifier was applied to local windows at various locations of the entire image to determine the probability (a scalar output between 0 and 1) of the presence of moth in a particular patch. Next, non-maximum suppression was performed, followed by thresholding, to retain only the windows with maximum local probability, and then only the patches over a certain probability were kept. The precision–recall area under the curve of about 0.934 was observed.

A mobile agricultural robot equipped with photography hardware and software for the detection of thrips (*Thysanoptera*), a pest related to strawberry plant, in greenhouses was developed in [145]. The robot moved along the rows of potted plants capturing flower images (RGB) using a digital camera (Canon EOS M, 18 MP, CMOS, Japan) mounted on the robot arm. The image processing was performed as follows: (i) the non-flower regions in the captured images were removed by applying the gamma operator. Next, histogram equalization and contrast stretching followed by intensity thresholding were used to remove the remaining background noise. Then, HSV components were extracted from the RGB values to serve as inputs for a SVM-based classifier with radial-basis kernel functions. The classifier was trained to not only detect pests but also identify thrips from other insects like houseflies, ants, and whiteflies. Moreover, since the shape and color of thrips also vary across larvae to adult stages, during the classification, two classes, one for larvae and another for adult were dedicated to thrips. Overall, a mean percent error (MPE) of about 2.5% was observed in the reported image processing system.

A human-vision-inspired method for pest detection in tea plants was reported in [144], where a collection of 10 categories of insect pests: *Locusta migratoria*, *Parasa lepida*, *Euproctis pseudoconspersa* Strand, *Empoasca flavescens*, *Spodoptera exigua*, *Chrysochus chinensis*, larva of *Laspeyresia pomonella*, larva of *S. exigua*, *Acrida cinerea*, and *L. pomonella* was investigated. For each category, about 40 to 70 sample images were collected from online resources. The identification method was based on computational models used to model human-vision system. First, the saliency using natural statistics (SUN) model was used to extract the region of interest. Then a well known model for object recognition with cortex-like mechanisms called Hierarchical Model and X (HMAX) [151] was extended by integrating scale invariant feature transform (SIFT) and non-negative sparse coding (NNSC) for improved rotational sensitivity of HMAX. Next, SIFT-HMAX model and local

configuration pattern algorithm were employed to extract the invariant features, which were then fed to the SVM-based classifier for recognition. The proposed method achieved a recognition rate of 85.5%.

An artificial neural network (ANN) coupled image processing system for identifying whiteflies (*Bemisa tabaci*) and thrips (*Frankliniella occidentalis*) on sticky traps in green house agriculture was presented in [147]. Solid yellow and blue colored traps (to minimize background effects) were digitized using Scoutbox sensor (Cropwatch Company, Wageningen, Netherlands), which consisted of a closed box, housing a digital camera to insulate light conditions. A total of 3185 images were acquired in RGB color format. First, the region of interest were identified on each trap based on pixel intensity histograms, where pixels with frequency of intensities above 10,000 (predetermined threshold) were set as background. Next, a binary image was created from each RGB channel, where pixels on the channel outside the background intensity range were classified as objects and only solid objects with an area from 50 to 2000 pixels were selected. Image segmentation was then performed by first converting the images to L*a*b* for yellow traps, and HSV format for blue traps. Automatic identification of the intensity threshold values was then implemented on each channel, and a logical conjunction operation was performed. Subsequently, the morphological features (area, convex area, eccentricity, equivalent diameter, major axis length, minor axis length, perimeter, centroid, solidity, and extent) were calculated for each region of pixels. Finally, a multi-layer feed-forward neural network consisting of a two-layer perceptron was trained for classification using 15 previously extracted features. The developed algorithm achieved precision of 0.96 and recall of 0.95 in whitefly identification, while precision of 0.92 and recall of 0.96 were obtained for thrip identification.

An imaging system powered by deep CNN (DCNN)-based classification for identifying five major diseases and pest (banana corm weevil) in banana plants was developed in [142], where the dataset comprised of about 18,000 images collected under field setting across Africa and Southern India. Images of various parts of the plant including the whole banana bunch, leaves, cut pseudostem, fruit bunch, and cut fruit were collected. Three different CNN architectures, ResNet50, InceptionV2, and MobileNetV1 were trained using the python deep learning library called Tensonflow. The diseases were grouped by plant parts, and a different model was trained for each plant part, where mean average precision (mAP)-based metric was used to measure the accuracy and effectiveness in object detection models:

$$mAP = \frac{1}{\#classes} \sum_1^{\#classes} \frac{\#TP}{\#TP + \#FP}. \quad (5)$$

In addition to mAP score, a confusion matrix (CM) for each selected model was also computed which gave an accuracy per disease (class), together with quantitative representation of the classes in which the model was mis-classified or confused. The experimental results achieved accuracy between 70 to 99%, where MobileNetV1-based architecture provided best results for banana corm weevil.

In addition to the aforementioned imaging-based pest detection methods, several other works have been reported in recent years including (i) a WSN for monitoring greenhouse insect pest, where the each wireless sensing node consisted of three core components: a Raspberry Pi 3 embedded system, a digital camera module, and add-on environmental sensors [140]. Sticky paper traps were imaged every ten minutes while humidity, temperature, and ambient light were also recorded. The RGB-to-L*a*b* color model conversion was performed, followed by an object segmentation by first removing the yellow sticky trap background using static binary thresholding. Selective blob detection was then performed on the pre-processed image to locate the centroids of the blobs (objects) in the image, where smaller (16 × 16 pixels; dirt) and larger (128 × 128 pixels; glare) blobs were removed. The cropped 128 × 128 RGB images obtained from the blob centroids were classified using an SVM-based classifier, where an average temporal accuracy for insect pest counting of 93% was achieved; (ii) a CNN-based architecture named PestNet, developed for large-scale multi-class pest detection [143]. An in-field imaging system was developed

consisting of a pest attracting light, and a pest collection tray fitted with a camera to collect pictures. 16 pest classes were considered, where an mAP score of 75.46% was achieved; (iii) a computer-vision technique for detecting aphids in wheat fields [148]. The original images were pre-processed with filtering to enhance the contrast and reduce noise followed by the extraction of histogram of oriented gradient (HOG) feature vectors which were subsequently used to establish SVM-based classification. Meanwhile, a maximally stable extremal region (MSER) algorithm was used on the original images to extract regions of interest and a trained SVM was used to identify aphids within the MSERs. An accuracy of 86.81% was achieved.

4.2. Acoustic Methods for Detecting Pests

One of the key ways pests/insects communicate with each other and their surroundings is through acoustic signals which can be used as signatures for detecting their presence. Studies on acoustic detection of pests have been reported since the early 1900s but have only gained momentum in the last two decades [152]. A bio-acoustic sensor for the early detection of the red palm weevil (RPW) was reported in [153], where the sensing device was composed of an audio probe inserted inside the palm tree trunk, with real-time processing circuit, wireless interface for periodic data transfer, and a solar panel/battery-based power supply system. A sound representative of the RPW larvae feeding action was chosen for detection, where the energy distribution (frequency domain representation) of the sound was used as the spectral fingerprint. A detection accuracy of about 90% was observed.

Several other recent works have been reported on acoustic pest detection including (i) an automated acoustic detection platform for detecting cicadid pest (*Quesada Gigas*; QG) in coffee plantations, where an SVM-based classifier was developed for distinguishing between background noise and QG's sound [154]. The sensing system was field deployable, costing around \$30 while exhibiting an accuracy of 96.41%; (ii) the detection of RPW, where piezoelectric microphones (inserted inside the tree trunk) were used to collect sound signals from a quarantined set of palm trees [155]. The larval feeding sounds: short "clicks" and "snaps" in the frequency range of 1 kHz to 8 kHz, and longer lasting sounds around 3 kHz were recorded. Manual and automated energy thresholds were used to identify pests, where an average true positive rate of 75% was achieved; (iii) the exploration of using active sound production of scarab beetle larvae (i.e., stridulations) for species-specific pest monitoring in soils [156].

Acoustic signature detection for monitoring pests is a non-invasive, real-time, continuous, low cost method which takes advantage of the developed microphone and signal processing technologies. However, the method has limited scope as only a small fraction of pests make species-specific sounds. Moreover, acoustic signaling-based methods are prone to interference from surroundings (natural and man-made) and in general, more studies are required to properly assess the practical in-field applicability of the method.

5. ET/VOCs Detection Methods for Monitoring Biotic Stress in Plants

Ethylene (ET) and other volatile organic compounds (VOCs) are common to plant response under both pathogenic and pest/insect related stresses, and so we discuss their detection in their own section here. The hormonal activity of ethylene spans a multitude of physiological plant processes including seed germination, fruition, and tissue senescence in case of phytopathogen and/or pest attacks. In addition to ET, several other VOCs play important roles in general crop health and physiological activities such as intra- and inter-plant communication [157], interaction with microbes [158], deterring herbivorous pests [36], and inducing defense responses [159]. This section describes key methodologies for the detection of ET/VOCs in agriculture, involving mass-spectroscopy and electronic nose technology (see Figure 10).

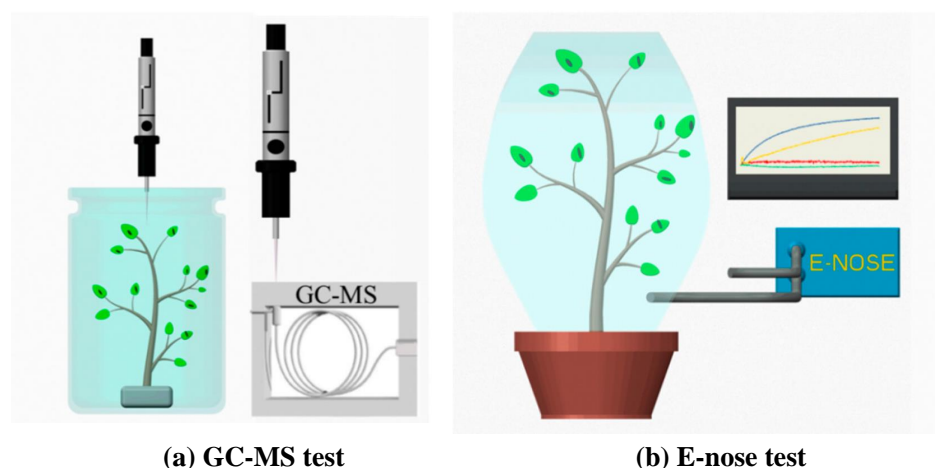


Figure 10. Schematic of an E-nose and a GC-MS-based system for VOC detection in plants [160].

Conventionally, gas analysis for plant VOCs is performed using standard analytical techniques like the well established gas chromatography-mass spectrometry (GC-MS) methods [161,162], and the relatively recent proton transfer reaction mass spectrometry (PTR-MS) method [163,164]. In GC-MS-based plant VOC analysis, the VOCs can be sampled from the airflow using an absorbent filter, which is then rinsed in a solvent and introduced in the heated GC-MS chamber, or alternatively, by headspace and solid-phase microextraction (HS-SPME), where the VOC are collected using a solvent coated fiber and directly introduced into the heated GC-MS column [161]. The gas molecules are then separated using a mass spectrometer (based on the molecular mass). Alternatively, PTR-MS works by ionizing the gas sample inside a drift tube by proton transfer (sourced from hydronium ion), where the fixed length of the drift tube provides a fixed reaction time for the ions as they pass along the tube into a mass spectrometer. The reaction time can be calculated from ion transfer properties to separate the gases, and the ion signal ratio (proton donor/proton acceptor) can be used to estimate the concentration of the analyte, and by combining reaction kinetics with mass spectrometry, both identity and quantity of individual organic gases can be obtained [164]. The main advantage of PTR-MS over GC-MS is its quick response. Although accurate and sensitive, GC-MS and PTR-MS require sophisticated equipment, and are thus better suited for laboratory-based testing.

With regards to portable ET/VOCs sensing, bio-mimetic *electronic nose* (E-nose) devices have emerged as a novel technology for gas detection. Several E-nose devices are commercially available [165–167], and have been employed for VOC detection. E-nose sensors consist of an array of chemical gas sensors coupled with transducers such as conductive polymers (polymers impregnated gas adsorbing materials resulting in resistance changes), Metal Oxide Semiconductor (MOS) device, piezoelectric/acoustic (changes in mass and resonance due to gas adsorption) devices, and optical/fluorescent sensors. The signal from the transducers is then processed using classification and/or pattern recognition algorithms. The sensor arrays can employ gas-specific sensing materials, deposited on the listed transducers, which selectively adsorb (or absorb) different gases. Gas-specific properties of several chemo-responsive materials for detecting various gases are summarized in [168]. Various studies have been reported on the use E-nose devices for plant-defense-related VOC monitoring, such as: (i) diagnosing Aphid-stressed tomato plants by first using GC-MS and identifying the VOCs emitted by the plant under stress including linalool, carveol, and nonane 2,2,4,4,6,8,8-heptamethyl and enhanced some terpene compounds (e.g., caryophyllene). Next, commercial E-nose devices were employed and a PCA-based algorithm was developed for portable VOC recognition with a classification accuracy of 86.7% [160]; (ii) application of E-nose for diagnosing grapevine crown gall disease (caused by *Agrobacterium vitis*) [169], where infected grapevine rootstock was sampled in glass tubes overnight and target VOCs were determined using HS-SPME coupled GC-MS. Next,

commercial E-nosed devices were employed and VOC data analysis was performed using PCA and linear discriminant analysis (LDA). An accuracy of 83.3% was achieved; (iii) an early detection of bacterial disease (fire blight caused by *Erwinia amylovora* and blossom blight caused by *Pseudomonas syringae*) in apple plants by monitoring VOC profiles [170], where the possible markers were identified using GC-MS and PTR-MS, while the application of commercial E-nose devices were assessed for portable operation demonstrating an accuracy of 75% using LDA-based data analysis.

In addition to the above-mentioned approaches, other ET/VOC sensing have also been reported including a smartphone-based VOC fingerprinting platform [171], where the diagnosis of late blight (caused by *Phytophthora infestans*) in tomato was demonstrated using leaf volatile emissions in the field. The handheld device integrated a disposable colorimetric sensor array consisting of plasmonic nanocolorants and chemo-responsive organic dyes to detect key plant volatiles at the ppm level within 1 min of reaction. Cysteine (Cys)-functionalized gold nanoparticles (AuNPs) or nanorods (AuNRs) were used as plasmonic aggregative colorants for specific recognition of gaseous (E)-2-hexenal, one of the main VOC markers emitted during *P. infestans* infection, with a detection limit of 0.4 ppm. Later, a multiplexed sensor array combining Cys-functionalized Au nanomaterials and conventional organic colorants were developed for the detection and differentiation of a variety of leaf volatiles, including three green leaf volatiles ((Z)-3-hexenal, 1-hexenal and (E)-2-hexenal), two phytohormones (methyl jasmonate and methyl salicylate), two characteristic late blight markers ((E)-2-hexenal and 2-phenylethanol), and three aromatic VOCs (benzaldehyde, 4-ethylguaiacol, and 4-ethylphenol) to demonstrate the capability for multiplexing.

A molecularly imprinted sol-gel (MISG)-based localized surface plasmon resonance (LSPR) sensor for detecting *cis-jasmone* (CJ), a plant VOC released in response to herbivore insect infestation, was reported in [172]. LSPR involves the interaction of metallic nanoparticles (NPs) with EM waves to induce plasmon oscillations at the NP surface and can be used as a transduction mechanism for observing changes in the local refractive index (RI). Gold nano-islands were fabricated on a glass substrate by vacuum sputtering followed by three dimensional imprints of CJ molecules with the MISG around the Au nano-islands. It was observed that MISGs containing the functional monomer trimethoxyphenylsilane at a 3:1 (v:v) ratio exhibited a higher sensitivity and selectivity among the imprints tested while a detection limit of 3.5 ppm in air was recorded.

A quartz crystal microbalance (QCM) gas sensor array based on MIPs for identifying wood borers infestation by monitoring terpene emissions from *Platyclusus orientalis* trunks was reported in [173]. MIPs were prepared using the methacrylic acid (MAA) polymer-matrix and four characteristic terpenes/VOCs (α -pinene, β -phellandrene, 3-carene, and cis-thujopsene) as template molecules for discriminating between *Semanotus bifasciatus* (Motschulsky) and *Phloeosinus aubei* Perris (Coleoptera: Scolytidae) infestations. The experimental set-up consisted of the four terpene MIPs-based QCM sensors inside a sealed chamber with inlet and outlet for gaseous samples. The QCM gas sensors measured the static headspace vapors of infested and uninfested trunks after generation for 24 h at 25 °C in uniform and suitable Tedlar bags where the absolute value of frequency shift based on the sensor response curve was defined as a feature. The response data were processed with PCA-LDA for visualization, and for discrimination/classification, an SVM-based architecture exhibited a satisfying response with an accuracy of 93.75%.

In another work, a plasmonic crystal-based optical gas sensor for ET, methanol, and ammonia detection was reported in [22], where the sensing surface consisted of a thin graphene-oxide (GO) layer deposited over a gold coated polymeric nanoposts. The working principle involved the gas adsorption by the GO layer modifying the refractive index of the plasmonic structure, resulting in a shift in the resonance wavelength of the surface plasmon polariton. To distinguish between the three types of gaseous species, an array of nanostructured sensors with varying thickness of GO were designed as the adsorption of different gases varies with GO thicknesses. A principle component analysis

(PCA)-based framework was employed to identify the three gases, where sensitivities of 0.6 pm/ppm, 3.2 pm/ppm, and 12.84 pm/ppm were observed for ET, methanol, and ammonia, respectively.

6. Application of Remote Sensing Technologies for Monitoring Biotic Stress in Plants

In general, the indirect plant disease and pest detection methods discussed so far in this article, particularly optical/imaging-based methods, have the potential to be integrated with a satellite and/or an airborne carrier and can broadly be classified as remote sensing (RS) methods. However, another class of active RS technology which includes radio detection and ranging (RADAR) and light detection and ranging (LiDAR) have also been applied towards sensing biotic stresses in plants. RADAR and LiDAR have traditionally been used as active methods for measuring distances by recording the travel time of emitted electromagnetic waves (radio waves for RADAR, and light/laser sources for LiDAR) reflection from a target object. Both RADAR and LiDAR inspired systems are applied in plant stress monitoring where some key research works are discussed here. The principle of operation of these systems involve capturing structural or morphological changes due to diseases and pests.

A ground-based LiDAR also known as terrestrial laser scanning (TLS) system for detecting basal stem rot (caused by white-rot fungus *Ganoderma boninense*) in oil palm canopies was reported in [174]. A total of 40 samples of oil palm trees at the age of nine-years-old (with heights between 10 to 11 meters) were selected and categorized into four disease levels: healthy/disease-free, mildly infected, moderately infected, and severely infected. The canopy biometrics were extracted using a TLS scanner which was mounted at a height of 1 m, and scans were performed from four different positions per palm to obtain a 3D image of the tree. The following parameters were analyzed: S200 (canopy strata at 200 cm from the top), S850 (canopy strata at 850 cm from the top), crown pixel (number of pixels inside the crown), frond angle (degree of angle between fronds), and frond number, where JMP software (SAS Institute, North Carolina, USA) was used to analyze the parameters using one-way analysis of variance (Kruskal–Wallis test). It was concluded that a linear model consisting of all the five parameters provides best results where an average accuracy of 80% for severity level classification and 86.67% for healthy–unhealthy classification was observed.

The capability of ground-penetrating radar (GPR) for evaluating the internal structure of tree trunks and detecting tree decay associated with emerging infectious diseases like Ash dieback, acute oak decline (AOD), and *Xylella fastidiosa* was reported in [175]. Measurements of tree trunk samples were taken using the Aladdin 2-GHz hand-held CO antenna from IDS GeoRadar (part of Hexagon). The core measurement principle involved digital reconstruction of the internal tree trunk structure based on Debye properties of the tree layers using the GPR system. Two data processing methodologies: modified Kirchhoff migration and reverse-time migration were applied for qualitative reconstruction. It was shown that the system was able to model the internal structure of the tree trunk, however, further investigation with a larger number of samples may be required to fully assess the proposed method's performance.

Other recent works on active RS-based methods for plant health monitoring include: (i) assessing the potential of dual-wavelength terrestrial LiDAR in early detection of bark beetle (*Ips typographus*) infestation [176]. Two terrestrial LiDAR systems (operating at 905 nm and 1550 nm) were used to measure 29 mature Norway spruce trees that showed mild to moderate symptoms. Several intensity metrics were derived from LiDAR data as inputs and LDA-based analysis was performed yielding an average classification accuracy of about 66%; (ii) evaluation of a GPR-based system for detection HLB infection in citrus trees by mapping their root architecture [177]. A GPR (TRU™ Model, Tree Radar, Inc., Silver Spring, MA, USA) equipped with a 1600 MHz antenna was mounted on a mobile cart to generate root morphology. The system was able to distinguish between dead and alive roots, based largely on the difference between their dielectric properties due

to water content variations. Qualitative efficacy of the developed system was shown and proposed to be of use in detecting soil-borne diseases in citrus trees; (iii) a bistatic LiDAR system mounted on a UAV/drone for monitoring strawberry canopies inside a greenhouse to detect symptoms of powdery mildew [178]. The principle of operation was based on detecting the changes in plant's carbon dioxide (CO₂) flux resulting from variation in the photosynthesis efficiency due to infection (CO₂ emissions decrease with disease progression). The developed system consisted of a static receiver that recorded the LiDAR signal (wavelength between 1572.38 nm to 1572.98 nm) from a transmitter mounted on the UAV, and the data was processed to determine the CO₂ flux based on the absorption characteristics above the crop canopies. The feasibility of the system was demonstrated; however, quantitative performance was not reported.

Overall, RADAR and LiDAR are well-developed technologies that have recently found use in plant biotic stress monitoring applications where extensive studies and experimentation is required to fully evaluate their capabilities. In addition to detecting plant stress, the active RS technology is employed in various other agro-ecosystem monitoring applications such as phenotyping plants based on their physical characteristic [179], visualizing plant structures like canopies and roots [180,181], and observing pest and/or herbivore behaviors [182]. In the present scenario, active RS-based systems exhibit a unique advantage in terms of feasibility for high-throughput automated drone/UAV-based agricultural sensing applications but often come with a high initial cost.

7. Discussion and Conclusions

This article described the current state of the sensing methodologies for monitoring biotic stresses in plants. Key methods for detecting phytopathogenic infections and herbivorous pest/insect infestations were reviewed, where the sensing mechanisms were described and key recent works reported. Phytopathogen sensing methods were categorized as direct pathogenic versus indirect plant response-based. Direct methods focused on identifying the pathogen directly using nucleic acid-based and pathogen-protein-based (serological/immunological) techniques such as PCR, RPA, LAMP, ELISA, LFIA, and immunosensors. Alternatively, indirect phytopathogen detection methods identified the plant defense related responses, both morphological and physiological. The plant response-based indirect disease detection techniques reported here include, imaging-based methods, fluorescence-based methods, spectroscopic techniques, phytohormone-level-based methods, and VOC-based sensors. Overall, direct pathogen detection methods offer excellent specificity, while the indirect ones provide a crop health analysis following plant immune responses. In general, indirect methods are relatively less labor intensive and hold greater scope for early detection under practical in-field setting. Monitoring primary defense-related phytohormone-levels may hold potential for identifying diseases, but more studies are required to discover and establish the essential correlations. Summarily, in the present state, direct and indirect methods for sensing pathogenic presence/stress can be used simultaneously and in conjunction to form a complete system for crop health monitoring and response, where the early signs of stress can be monitored using plant response-based indirect approaches, while further analysis can be performed using the direct pathogen identification methods.

The article further surveyed the pest/insects detection methods, that included machine-vision-based methods, pest acoustic-signal detection, and VOC sensing-based methods. In the case of pest attacks, the density of a specific infestation is a critical stress parameter, and therefore the sensing techniques largely focus on spatio-temporal count and identity of the pest. The common steps involved in imaging-based detection are photographing the insect prior to analysis, either directly or on the plant tissue or using specially designed traps, and then classify for obtaining insect species and count. Several systems have been developed, however, continuous efforts are being directed towards improving the accuracy and specificity of imaging-based methods. Acoustic-signaling-based approaches, on the other hand, rely on detecting the infestation depending on the sounds emitted by the

insects while communicating or interacting with their environment. These methods are applicable only to a small subset of pests and require further studies in order to develop robust in-field monitoring systems.

Monitoring VOCs have also been reported as early indicators of biotic stresses in plants, however clear distinction between VOC emissions in plants due to specific pest and/or pathogen attacks are not completely understood. However, continuous progress is being made towards forming functional VOC-stress correlations as well as developing VOC detection methods. The approaches discussed here include: analytical methods (GC-MS), E-nose devices, and other approaches (biosensing and optical). Among these, E-nose-based sensors have emerged as an effective technology offering great potential for in-field operation where efforts are being directed towards effective sampling procedures, improving accuracy and specificity, and developing long-term continuous monitoring systems. Where E-nose devices focus on detecting common agriculturally and environmentally important gases, biosensing and optical methods aim to identify specific VOC emissions like terpenes, and other gaseous metabolites (for example cis-jasmone, and methyl salicylate).

Additionally, active RS technologies like RADAR and LiDAR also find use in applications for sensing biotic stress in plants. These technologies are fairly well-known and are being progressively used in various aspects of agriculture such as recording canopy, plant height and root structures, and phenotyping applications. While both RADAR- and LiDAR-based systems commonly provide morphological information, LiDAR may have the potential to record plant's physiological parameters like, water content and CO₂ flux. Overall, testing the application of active RS technologies to provide plant stress-related information is a rapidly progressing area of research that may soon enable large-scale automated crop and forest health monitoring systems.

8. Future Prospects and Research Directions for Monitoring Biotic Stress in Plants

In the present scenario, there is great scope for making significant improvements in agricultural output efficiencies by reducing crop losses to meet the present and future demands of humanity. Use of technology in farming practices is gaining rapid momentum where reportedly, the global technology market in agriculture is expected to grow at a compound annual growth rate (CAGR) of 14.1% from 2019 to reach \$34.9 billion by 2027 [183].

As described in this article, there are a variety of technologies available for detecting and identifying the different types of biotic stresses in crops. However, to increase the applicability and adoption of the stress monitoring technologies future efforts may be directed towards first, developing functional, easy-to-use, and reliable sensing methods for predictive/pre-symptomatic monitoring as well as accurate post-symptomatic diagnosis for enabling effective measures to minimize losses while reducing the use of harmful chemicals. Second, it is known that biotic stressors vary with plant species as well as locations across the globe, therefore, effective site and species specific strategies for standardized protocols and minimal sampling needs to be developed for both generalized as well as specific plant health monitoring that are cost-effective, portable, and high impact. Thirdly, in addition to water, nutrient, and environmental sensing data, crop stress monitoring must also be considered as an important parameter in agricultural management to accurately access the crop needs leading to sustainability through precision in agriculture. Finally, the overall development of the methodologies for monitoring biotic stress in plants stem from studies focusing on understanding their physiological processes and defense mechanisms hence, continuous progress is required in improving our knowledge about the *rules of life and survival* across the diverse *flora* on earth.

Author Contributions: Conceptualization, B.K.; methodology, B.K.; formal analysis, B.K.; investigation, B.K.; resources, B.K.; writing—original draft preparation, B.K.; writing—review and editing, B.K. and R.K.; visualization, B.K.; supervision, R.K.; project administration, R.K.; funding acquisition, R.K. All authors have read and agreed to the published version of the manuscript.

Funding: The work was supported in part by the National Science Foundation under the Grants CCF-1331390, ECCS-1509420, PFI-1602089, and CSSI-2004766.

Institutional Review Board Statement: Not applicable.

Informed Consent Statement: Not applicable.

Conflicts of Interest: The authors declare no conflict of interest.

References

1. World Population Projected to Reach 9.8 billion in 2050, and 11.2 billion in 2100. Available Online: <https://www.un.org/development/desa/en/news/population/world-population-prospects-2017.html> (accessed on 25 July 2020).
2. Elferink, M.; Schierhorn, F. Global Demand for Food Is Rising. Can We Meet It? Available Online: <https://hbr.org/2016/04/global-demand-for-food-is-rising-can-we-meet-it> (accessed on 2 December 2020).
3. Savary, S.; Willocquet, L.; Pethybridge, S.J.; Esker, P.; McRoberts, N.; Nelson, A. The global burden of pathogens and pests on major food crops. *Nat. Ecol. Evol.* **2019**, *3*, 430–439. [CrossRef] [PubMed]
4. Global Burden of Crop Loss. Available online: <https://www.cabi.org/projects/global-burden-of-crop-loss/> (accessed on 2 December 2020).
5. Xu, Z.; Dong, L.; Kumar, R. Electrophoretic Soil Nutrient Sensor for Agriculture. U.S. Patent 10,564,122, 18 February 2020.
6. Kumar, R.; Weber, R.J.; Pandey, G. Low RF-Band Impedance Spectroscopy Based Sensor for In-Situ, Wireless Soil Sensing. U.S. Patent 10,073,074, 18 September 2018.
7. Pandey, G.; Weber, R.J.; Kumar, R. Agricultural cyber-physical system: In-situ soil moisture and salinity estimation by dielectric mixing. *IEEE Access* **2018**, *6*, 43179–43191. [CrossRef]
8. Xu, Z.; Wang, X.; Weber, R.J.; Kumar, R.; Dong, L. Nutrient sensing using chip scale electrophoresis and in situ soil solution extraction. *IEEE Sens. J.* **2017**, *17*, 4330–4339. [CrossRef]
9. Ali, M.A.; Jiang, H.; Mahal, N.K.; Weber, R.J.; Kumar, R.; Castellano, M.J.; Dong, L. Microfluidic impedimetric sensor for soil nitrate detection using graphene oxide and conductive nanofibers enabled sensing interface. *Sens. Actuators B Chem.* **2017**, *239*, 1289–1299. [CrossRef]
10. Xu, Z.; Wang, X.; Weber, R.J.; Kumar, R.; Dong, L. Microfluidic eletrophoretic ion nutrient sensor. In Proceedings of the 2016 IEEE SENSORS, Orlando, FL, USA, 30 October–3 November 2016; pp. 1–3.
11. Pandey, G.; Wang, K.N.; Kumar, R.; Weber, R.J. Employing a metamaterial inspired small antenna for sensing and transceiving data in an underground soil sensor equipped with a GUI for end-user. In Proceedings of the 2014 IEEE International Conference on Systems, Man, and Cybernetics (SMC), San Diego, CA, USA, 5–8 October 2014; pp. 3423–3428.
12. Britz, B.; Ng, E.; Jiang, H.; Xu, Z.; Kumar, R.; Dong, L. Smart nitrate-selective electrochemical sensors with electrospun nanofibers modified microelectrode. In Proceedings of the 2014 IEEE International Conference on Systems, Man, and Cybernetics (SMC), San Diego, CA, USA, 5–8 October 2014; pp. 3419–3422.
13. Pandey, G.; Kumar, R.; Weber, R.J. A low profile, low-RF band, small antenna for underground, in-situ sensing and wireless energy-efficient transmission. In Proceedings of the 11th IEEE International Conference on Networking, Sensing and Control, Miami, FL, USA, 7–9 April 2014; pp. 179–184.
14. Pandey, G.; Kumar, R.; Weber, R.J. Design and implementation of a self-calibrating, compact micro strip sensor for in-situ dielectric spectroscopy and data transmission. In Proceedings of the SENSORS, Baltimore, MD, USA, 3–6 November 2013; pp. 1–4.
15. Pandey, G.; Kumar, R.; Weber, R.J. Real time detection of soil moisture and nitrates using on-board in-situ impedance spectroscopy. In Proceedings of the 2013 IEEE International Conference on Systems, Man, and Cybernetics, Manchester, UK, 13–16 October 2013; pp. 1081–1086.
16. Pandey, G.; Kumar, R.; Weber, R.J. Determination of soil ionic concentration using impedance spectroscopy. In *Sensing Technologies for Global Health, Military Medicine, and Environmental Monitoring III*; International Society for Optics and Photonics: Bellingham, WA, USA, 2013; Volume 8723, p. 872317.
17. Pandey, G.; Kumar, R.; Weber, R.J. A multi-frequency, self-calibrating, in-situ soil sensor with energy efficient wireless interface. In *Sensing for Agriculture and Food Quality and Safety V*; International Society for Optics and Photonics: Bellingham, WA, USA, 2013; Volume 8721, p. 87210V.
18. Kumar, R.; Tabassum, S.; Dong, L. Nano-Patterning Methods Including:(1) Patterning of Nanophotonic Structures at Optical Fiber Tip for Refractive Index Sensing and (2) Plasmonic Crystal Incorporating Graphene Oxide Gas Sensor for Detection of Volatile Organic Compounds. U.S. Patent 10,725,373, 28 July 2020.
19. Kashyap, B.; Kumar, R. Sensing Methodologies in Agriculture for Soil Moisture and Nutrient Monitoring. *IEEE Access* **2021**, *9*, 14095–14121. [CrossRef]

20. Tabassum, S.; Dong, L.; Kumar, R. Determination of dynamic variations in the optical properties of graphene oxide in response to gas exposure based on thin-film interference. *Opt. Express* **2018**, *26*, 6331–6344. [[CrossRef](#)]
21. Tabassum, S.; Kumar, R.; Dong, L. Nanopatterned optical fiber tip for guided mode resonance and application to gas sensing. *IEEE Sens. J.* **2017**, *17*, 7262–7272. [[CrossRef](#)]
22. Tabassum, S.; Kumar, R.; Dong, L. Plasmonic Crystal-Based Gas Sensor Toward an Optical Nose Design. *IEEE Sens. J.* **2017**, *17*, 6210–6223. [[CrossRef](#)]
23. Tabassum, S.; Kumar, R. Selective Detection of Ethylene Using a Fiber-Optic Guided Mode Resonance Device: In-Field Crop/Fruit Diagnostics. In *CLEO: Applications and Technology*; Optical Society of America: Washington, DC, USA, 2020; p. ATu4I-6.
24. Kashyap, B.; Kumar, R. Salicylic acid (SA) detection using bi-enzyme microfluidic electrochemical sensor. In *Smart Biomedical and Physiological Sensor Technology XV*; Cullum, B.M., Kiehl, D., McLamore, E.S., Eds.; International Society for Optics and Photonics, SPIE: Bellingham, WA, USA, 2018; Volume 10662, pp. 97–103.
25. Kashyap, B.; Kumar, R. Bio-agent free electrochemical detection of Salicylic acid. In Proceedings of the 2019 IEEE SENSORS, Montreal, QC, Canada, 27–30 October 2019; pp. 1–4.
26. Tabassum, S.; Wang, Q.; Wang, W.; Oren, S.; Ali, M.A.; Kumar, R.; Dong, L. Plasmonic crystal gas sensor incorporating graphene oxide for detection of volatile organic compounds. In Proceedings of the 2016 IEEE 29th International Conference on Micro Electro Mechanical Systems (MEMS), Shanghai, China, 24–28 January 2016; pp. 913–916.
27. Bhar, A.; Kumar, R.; Qi, Z.; Malone, R. Coordinate descent based agricultural model calibration and optimized input management. *Comput. Electron. Agric.* **2020**, *172*, 105353. [[CrossRef](#)]
28. Bhar, A.; Kumar, R.; Malone, R.W. Comparing a Simple Carbon Nitrogen Model with Complex RZWQM Model. In Proceedings of the 2019 ASABE Annual International Meeting, American Society of Agricultural and Biological Engineers, Boston, MA, USA, 7–10 July 2019; p. 1.
29. Bhar, A.; Kumar, R. Model-Predictive Real-Time Fertilization and Irrigation Decision-Making Using RZWQM. In Proceedings of the 2019 ASABE Annual International Meeting, American Society of Agricultural and Biological Engineers, Boston, MA, USA, 7–10 July 2019; p. 1.
30. Erb, M.; Meldau, S.; Howe, G.A. Role of phytohormones in insect-specific plant reactions. *Trends Plant Sci.* **2012**, *17*, 250–259. [[CrossRef](#)]
31. Freeman, B.C.; Beattie, G. An Overview of Plant Defenses against Pathogens and Herbivores. *Plant Health Instr.* **2008**. [[CrossRef](#)]
32. Spoel, S.H.; Dong, X. How do plants achieve immunity?: Defence without specialized immune cells. *Nat. Rev. Immunol.* **2012**, *12*, 89–100. [[CrossRef](#)]
33. Pel, M.J.C.; Pieterse, C.M.J. Microbial recognition and evasion of host immunity. *J. Exp. Bot.* **2012**, *64*, 1237–1248. [[CrossRef](#)]
34. Miller, R.N.G.; Costa Alves, G.S.; Van Sluys, M.A. Plant immunity: Unravelling the complexity of plant responses to biotic stresses. *Ann. Bot.* **2017**, *119*, 681–687. [[CrossRef](#)]
35. Wu, S.; Shan, L.; He, P. Microbial signature-triggered plant defense responses and early signaling mechanisms. *Plant Sci.* **2014**, *228*, 118–126. [[CrossRef](#)]
36. War, A.R.; Paulraj, M.G.; Ahmad, T.; Buhroo, A.A.; Hussain, B.; Ignacimuthu, S.; Sharma, H.C. Mechanisms of plant defense against insect herbivores. *Plant Signal. Behav.* **2012**, *7*, 1306–1320. [[CrossRef](#)]
37. Ross, A. Systemic acquired resistance induced by localized virus infections in plants. *Virology* **1961**, *14*, 340–358. [[CrossRef](#)]
38. Vos, I.A.; Pieterse, C.M.J.; van Wees, S.C.M. Costs and benefits of hormone-regulated plant defences. *Plant Pathol.* **2013**, *62*, 43–55. [[CrossRef](#)]
39. Berens, M.L.; Wolinska, K.W.; Spaepen, S.; Ziegler, J.; Nobori, T.; Nair, A.; Krüler, V.; Winkelmüller, T.M.; Wang, Y.; Mine, A.; Becker, D.; Garrido-Oter, R.; Schulze-Lefert, P.; Tsuda, K. Balancing trade-offs between biotic and abiotic stress responses through leaf age-dependent variation in stress hormone cross-talk. *Proc. Natl. Acad. Sci. USA* **2019**, *116*, 2364–2373. [[CrossRef](#)]
40. Mao, Y.B.; Liu, Y.Q.; Chen, D.Y.; Chen, F.Y.; Fang, X.; Hong, G.J.; Wang, L.J.; Wang, J.W.; Chen, X.Y. Jasmonate response decay and defense metabolite accumulation contributes to age-regulated dynamics of plant insect resistance. *Nature Communications*. *Nat. Commun.* **2017**, *8*, 13925. [[CrossRef](#)]
41. Li, N.; Han, X.; Feng, D.; Yuan, D.; Huang, L.J. Signaling Crosstalk between Salicylic Acid and Ethylene/Jasmonate in Plant Defense: Do We Understand What They Are Whispering? *Int. J. Mol. Sci.* **2019**, *20*, 671. [[CrossRef](#)]
42. Xu, T.; Yao, Z.; Liu, J.; Zhang, H.; Din, G.M.U.; Zhao, S.; Chen, W.; Liu, T.; Gao, L. Development of droplet digital PCR for the detection of *Tilletia laevis*, which causes common bunt of wheat, based on the SCAR marker derived from ISSR and real-time PCR. *Sci. Rep.* **2020**, *10*, 16106. [[CrossRef](#)]
43. Aglietti, C.; Luchi, N.; Pepori, A.L.; Bartolini, P.; Pecori, F.; Raio, A.; Capretti, P.; Santini, A. Real-time loop-mediated isothermal amplification: an early-warning tool for quarantine plant pathogen detection. *AMB Express* **2019**, *9*, 50. [[CrossRef](#)]
44. Ristaino, J.B.; Saville, A.C.; Paul, R.; Cooper, D.C.; Wei, Q. Detection of *Phytophthora infestans* by Loop-Mediated Isothermal Amplification, Real-Time LAMP, and Droplet Digital PCR. *Plant Dis.* **2020**, *104*, 708–716. [[CrossRef](#)]
45. Charlermoj, R.; Himananto, O.; Seepiban, C.; Kumposiri, M.; Warin, N.; Oplatowska, M.; Gajanandana, O.; Grant, I.R.; Karoonuthaisiri, N.; Elliott, C.T. Multiplex Detection of Plant Pathogens Using a Microsphere Immunoassay Technology. *PLoS ONE* **2013**, *8*, 1–11. [[CrossRef](#)]
46. Panferov, V.G.; Safenkova, I.V.; Byzova, N.A.; Varitsev, Y.A.; Zherdev, A.V.; Dzantiev, B.B. Silver-enhanced lateral flow immunoassay for highly-sensitive detection of potato leafroll virus. *Food Agric. Immunol.* **2018**, *29*, 445–457. [[CrossRef](#)]

47. Song, S.; Liu, N.; Zhao, Z.; Njumbe Ediage, E.; Wu, S.; Sun, C.; De Saeger, S.; Wu, A. Multiplex Lateral Flow Immunoassay for Mycotoxin Determination. *Anal. Chem.* **2014**, *86*, 4995–5001. [[CrossRef](#)]
48. Anfossi, L.; Di Nardo, F.; Giovannoli, C.; Passini, C.; Baggiani, C. Increased sensitivity of lateral flow immunoassay for ochratoxin A through silver enhancement. *Anal. Bioanal. Chem.* **2013**, *405*, 9859–9867. [[CrossRef](#)]
49. Lin, H.Y.; Huang, C.H.; Lu, S.H.; Kuo, I.T.; Chau, L.K. Direct detection of orchid viruses using nanorod-based fiber optic particle plasmon resonance immunosensor. *Biosens. Bioelectron.* **2014**, *51*, 371–378. [[CrossRef](#)] [[PubMed](#)]
50. Berto, M.; Vecchi, E.; Baiamonte, L.; Condò, C.; Sensi, M.; Di Lauro, M.; Sola, M.; De Stradis, A.; Biscarini, F.; Minafra, A.; Bortolotti, C.A. Label free detection of plant viruses with organic transistor biosensors. *Sens. Actuators B Chem.* **2019**, *281*, 150–156. [[CrossRef](#)]
51. Mullis, K.B. The Unusual Origin of the Polymerase Chain Reaction. *Sci. Am.* **1990**, *262*, 56–65. [[CrossRef](#)] [[PubMed](#)]
52. WARD, E.; FOSTER, S.J.; FRAAIJE, B.A.; MCCARTNEY, H.A. Plant pathogen diagnostics: Immunological and nucleic acid-based approaches. *Ann. Appl. Biol.* **2004**, *145*, 1–16. [[CrossRef](#)]
53. Athman, A.; Tanz, S.K.; Conn, V.M.; Jordans, C.; Mayo, G.M.; Ng, W.W.; Burton, R.A.; Conn, S.J.; Gilliam, M. Protocol: A fast and simple in situ PCR method for localising gene expression in plant tissue. *Plant Methods* **2014**, *10*, 29. [[CrossRef](#)] [[PubMed](#)]
54. Lee, M.H.; Song, K.Y.; Hwang, H.J.; Kim, J.H.; Hwang, I. Development of fast and sensitive protocols for the detection of viral pathogens using a small portable convection PCR platform. *Mol. Biol. Rep.* **2019**, *46*, 5073–5077. [[CrossRef](#)]
55. Martinelli, F.; Scalenghe, R.; Davino, S.; Panno, S.; Scuderi, G.; Ruisi, P.; Villa, P.; Stroppiana, D.; Boschetti, M.; Goulart, L.R.; Davis, C.E.; Dandekar, A.M. Advanced methods of plant disease detection. A review. *Agron. Sustain. Dev.* **2015**, *35*, 1–25. [[CrossRef](#)]
56. Paul, R.; Saville, A.C.; Hansel, J.C.; Ye, Y.; Ball, C.; Williams, A.; Chang, X.; Chen, G.; Gu, Z.; Ristaino, J.B.; Wei, Q. Extraction of Plant DNA by Microneedle Patch for Rapid Detection of Plant Diseases. *ACS Nano* **2019**, *13*, 6540–6549. [[CrossRef](#)]
57. Koo, C.; Malapi-Wight, M.; Kim, H.S.; Cifci, O.S.; Vaughn-Diaz, V.L.; Ma, B.; Kim, S.; Abdel-Raziq, H.; Ong, K.; Jo, Y.K.; et al. Development of a Real-Time Microchip PCR System for Portable Plant Disease Diagnosis. *PLoS ONE* **2013**, *8*, 1–11. [[CrossRef](#)]
58. What Is a Cq (Ct) Value? Available Online: <https://bitesizebio.com/24581/what-is-a-ct-value/> (accessed on 15 December 2020).
59. Hajizadeh, M.; Navarro, B.; Bashir, N.S.; Torchetti, E.M.; Di Serio, F. Development and validation of a multiplex RT-PCR method for the simultaneous detection of five grapevine viroids. *J. Virol. Methods* **2012**, *179*, 62–69. [[CrossRef](#)]
60. Sanzani, S.M.; Li Destri Nicosia, M.G.; Faedda, R.; Cacciola, S.O.; Schena, L. Use of Quantitative PCR Detection Methods to Study Biocontrol Agents and Phytopathogenic Fungi and Oomycetes in Environmental Samples. *J. Phytopathol.* **2014**, *162*, 1–13. [[CrossRef](#)]
61. Duressa, D.; Rauscher, G.; Koike, S.T.; Mou, B.; Hayes, R.J.; Maruthachalam, K.; Subbarao, P.V.; Klosterman, S.J. A Real-Time PCR Assay for Detection and Quantification of *Verticillium dahliae* in Spinach Seed. *Phytopathology* **2012**, *102*, 443–451. [[CrossRef](#)]
62. DeShields, J.B.; Bomberger, R.A.; Woodhall, J.W.; Wheeler, D.L.; Moroz, N.; Johnson, D.A.; Tanaka, K. On-Site Molecular Detection of Soil-Borne Phytopathogens Using a Portable Real-Time PCR System. *J. Vis. Exp.* **2018**, *132*, e56891. [[CrossRef](#)]
63. Londoño, M.A.; Harmon, C.L.; Polston, J.E. Evaluation of recombinase polymerase amplification for detection of begomoviruses by plant diagnostic clinics. *Virol. J.* **2016**, *13*, 48. [[CrossRef](#)]
64. Lobato, I.M.; O’Sullivan, C.K. Recombinase polymerase amplification: Basics, applications and recent advances. *TrAC Trends Anal. Chem.* **2018**, *98*, 19–35. [[CrossRef](#)]
65. Lau, H.Y.; Wu, H.; Wee, E.J.H.; Trau, M.; Wang, Y.; Botella, J.R. Specific and Sensitive Isothermal Electrochemical Biosensor for Plant Pathogen DNA Detection with Colloidal Gold Nanoparticles as Probes. *Sci. Rep.* **2017**, *7*, 38896. [[CrossRef](#)]
66. Yu, J.; Shen, D.; Dai, T.; Lu, X.; Xu, H.; Dou, D. Rapid and equipment-free detection of *Phytophthora capsici* using lateral flow strip-based recombinase polymerase amplification assay. *Letts. Appl. Microbiol.* **2019**, *69*, 64–70. [[CrossRef](#)]
67. Zou, Y.; Mason, M.G.; Wang, Y.; Wee, E.; Turni, C.; Blackall, P.J.; Trau, M.; Botella, J.R. Nucleic acid purification from plants, animals and microbes in under 30 seconds. *PLoS Biol.* **2017**, *15*, 1–22. [[CrossRef](#)]
68. Strayer-Scherer, A.; Jones, J.B.; Paret, M.L. Recombinase Polymerase Amplification Assay for Field Detection of Tomato Bacterial Spot Pathogens. *Phytopathology* **2019**, *109*, 690–700. [[CrossRef](#)]
69. Zhang, S.; Ravelonandro, M.; Russell, P.; McOwen, N.; Briard, P.; Bohannon, S.; Vrient, A. Rapid diagnostic detection of plum pox virus in Prunus plants by isothermal AmplifyRP® using reverse transcription-recombinase polymerase amplification. *J. Virol. Methods* **2014**, *207*, 114–120. [[CrossRef](#)]
70. Zeng, R.; Luo, J.; Gao, S.; Xu, L.; Song, Z.; Dai, F. Rapid detection of Cucumber green mottle mosaic virus by reverse transcription recombinase polymerase amplification. *Mol. Cell. Probes* **2019**, *43*, 84–85. [[CrossRef](#)]
71. Mekuria, T.A.; Zhang, S.; Eastwell, K.C. Rapid and sensitive detection of Little cherry virus 2 using isothermal reverse transcription-recombinase polymerase amplification. *J. Virol. Methods* **2014**, *205*, 24–30. [[CrossRef](#)]
72. Tomita, N.; Mori, Y.; Kanda, H.; Notomi, T. Loop-mediated isothermal amplification (LAMP) of gene sequences and simple visual detection of products. *Nat. Protoc.* **2008**, *3*, 877–882. [[CrossRef](#)] [[PubMed](#)]
73. Wong, Y.P.; Othman, S.; Lau, Y.L.; Radu, S.; Chee, H.Y. Loop-mediated isothermal amplification (LAMP): A versatile technique for detection of micro-organisms. *J. Appl. Microbiol.* **2018**, *124*, 626–643. [[CrossRef](#)] [[PubMed](#)]
74. Karakkat, B.B.; Hockemeyer, K.; Franchett, M.; Olson, M.; Mullenberg, C.; Koch, P.L. Detection of root-infecting fungi on cool-season turfgrasses using loop-mediated isothermal amplification and recombinase polymerase amplification. *J. Microbiol. Methods* **2018**, *151*, 90–98. [[CrossRef](#)] [[PubMed](#)]

75. Plant Pathogen Tests—Creative Diagnostics. Available online: <https://www.creative-diagnostics.com/plant-pathogen-elisa-kits.htm> (accessed on 16 December 2020).
76. Agdia—ELISA. Available online: <https://orders.agdia.com/pathogen-tests/elisa> (accessed on 16 December 2020).
77. Bio-Rad. What Is ELISA?—An Introduction to ELISA. Available online: <https://www.bio-rad-antibodies.com/an-introduction-to-elisa.html> (accessed on 16 December 2020).
78. Estrela, P.; Koczula, K.; Gallotta, A. Lateral flow assays. *Essays Biochem.* **2016**, *60*, 111–120. [[CrossRef](#)]
79. Razo, S.C.; Panferov, V.G.; Safenkova, I.V.; Varitsev, Y.A.; Zherdev, A.V.; Dzantiev, B.B. Double-enhanced lateral flow immunoassay for potato virus X based on a combination of magnetic and gold nanoparticles. *Anal. Chim. Acta* **2018**, *1007*, 50–60. [[CrossRef](#)]
80. Chen, Y.; Chen, Q.; Han, M.; Zhou, J.; Gong, L.; Niu, Y.; Zhang, Y.; He, L.; Zhang, L. Development and optimization of a multiplex lateral flow immunoassay for the simultaneous determination of three mycotoxins in corn, rice and peanut. *Food Chem.* **2016**, *213*, 478–484. [[CrossRef](#)]
81. Haji-Hashemi, H.; Habibi, M.M.; Safarnejad, M.R.; Norouzi, P.; Ganjali, M.R. Label-free electrochemical immunosensor based on electrodeposited Prussian blue and gold nanoparticles for sensitive detection of citrus bacterial canker disease. *Sens. Actuators B Chem.* **2018**, *275*, 61–68. [[CrossRef](#)]
82. Riberi, W.I.; Tarditto, L.V.; Zon, M.A.; Arévalo, F.J.; Fernández, H. Development of an electrochemical immunosensor to determine zearalenone in maize using carbon screen printed electrodes modified with multi-walled carbon nanotubes/polyethyleneimine dispersions. *Sens. Actuators B Chem.* **2018**, *254*, 1271–1277. [[CrossRef](#)]
83. Zhao, Y.; Liu, L.; Kong, D.; Kuang, H.; Wang, L.; Xu, C. Dual Amplified Electrochemical Immunosensor for Highly Sensitive Detection of *Pantoea stewartii* subsp. *stewartii*. *ACS Appl. Mater. Interfaces* **2014**, *6*, 21178–21183. [[CrossRef](#)]
84. Hashemi Tameh, M.; Primiceri, E.; Chiriaco, M.S.; Poltronieri, P.; Bahar, M.; Maruccio, G. Pectobacterium atrosepticum Biosensor for Monitoring Blackleg and Soft Rot Disease of Potato. *Biosensors* **2020**, *10*, 64. [[CrossRef](#)]
85. Zeng, C.; Huang, X.; Xu, J.; Li, G.; Ma, J.; Ji, H.F.; Zhu, S.; Chen, H. Rapid and sensitive detection of maize chlorotic mottle virus using surface plasmon resonance-based biosensor. *Anal. Biochem.* **2013**, *440*, 18–22. [[CrossRef](#)]
86. Hallau, L.; Neumann, M.; Klatt, B.; Kleinhenz, B.; Klein, T.; Kuhn, C.; Röhrig, M.; Bauckhage, C.; Kersting, K.; Mahlein, A.K.; et al. Automated identification of sugar beet diseases using smartphones. *Plant Pathol.* **2018**, *67*, 399–410. [[CrossRef](#)]
87. Johannes, A.; Picon, A.; Alvarez-Gila, A.; Echazarra, J.; Rodriguez-Vaamonde, S.; Navajas, A.D.; Ortiz-Barredo, A. Automatic plant disease diagnosis using mobile capture devices, applied on a wheat use case. *Comput. Electron. Agric.* **2017**, *138*, 200–209. [[CrossRef](#)]
88. Petrellis, N. A smart phone image processing application for plant disease diagnosis. In Proceedings of the 2017 6th International Conference on Modern Circuits and Systems Technologies (MOCASST), Thessaloniki, Greece, 4–6 May 2017; pp. 1–4.
89. Mohanty, S.P.; Hughes, D.P.; Salathé, M. Using Deep Learning for Image-Based Plant Disease Detection. *Front. Plant Sci.* **2016**, *7*, 1419. [[CrossRef](#)]
90. Barbedo, J.G.A.; Koenigkan, L.V.; Santos, T.T. Identifying multiple plant diseases using digital image processing. *Biosyst. Eng.* **2016**, *147*, 104–116. [[CrossRef](#)]
91. Schor, N.; Bechar, A.; Ignat, T.; Dombrovsky, A.; Elad, Y.; Berman, S. Robotic Disease Detection in Greenhouses: Combined Detection of Powdery Mildew and Tomato Spotted Wilt Virus. *IEEE Robot. Autom. Lett.* **2016**, *1*, 354–360. [[CrossRef](#)]
92. Zhou, R.; Kaneko, S.; Tanaka, F.; Kayamori, M.; Shimizu, M. Image-based field monitoring of *Cercospora* leaf spot in sugar beet by robust template matching and pattern recognition. *Comput. Electron. Agric.* **2015**, *116*, 65–79. [[CrossRef](#)]
93. Pourreza, A.; Lee, W.S.; Ehsani, R.; Schueller, J.K.; Raveh, E. An optimum method for real-time in-field detection of Huanglongbing disease using a vision sensor. *Comput. Electron. Agric.* **2015**, *110*, 221–232. [[CrossRef](#)]
94. Lloret, J.; Bosch, I.; Sendra, S.; Serrano, A. A Wireless Sensor Network for Vineyard Monitoring That Uses Image Processing. *Sensors* **2011**, *11*, 6165–6196. [[CrossRef](#)]
95. Moghadam, P.; Ward, D.; Goan, E.; Jayawardena, S.; Sikka, P.; Hernandez, E. Plant Disease Detection Using Hyperspectral Imaging. In Proceedings of the 2017 International Conference on Digital Image Computing: Techniques and Applications (DICTA), Sydney, NSW, Australia, 29 November–1 December 2017; pp. 1–8.
96. Mishra, P.; Asaari, M.S.M.; Herrero-Langreo, A.; Lohumi, S.; Diezma, B.; Scheunders, P. Close range hyperspectral imaging of plants: A review. *Biosyst. Eng.* **2017**, *164*, 49–67. [[CrossRef](#)]
97. Abdulridha, J.; Ampatzidis, Y.; Kakarla, S.C.; Roberts, P. Detection of target spot and bacterial spot diseases in tomato using UAV-based and benchtop-based hyperspectral imaging techniques. *Precis. Agric.* **2020**, *21*, 955–978. [[CrossRef](#)]
98. Wang, Dongyi, V.R.; Holmes, M.; Seibel, G.; Bechar, A.; Nof, S.; Tao, Y. Early Detection of Tomato Spotted Wilt Virus by Hyperspectral Imaging and Outlier Removal Auxiliary Classifier Generative Adversarial Nets (OR-AC-GAN). *Sci. Rep.* **2019**, *9*, 4377. [[CrossRef](#)]
99. Nagasubramanian, K.; Jones, S.; Singh, A.K.; Sarkar, S.; Singh, A.; Ganapathysubramanian, B. Plant disease identification using explainable 3D deep learning on hyperspectral images. *Plant Methods* **2019**, *15*, 98. [[CrossRef](#)]
100. Zhang, X.; Han, L.; Dong, Y.; Shi, Y.; Huang, W.; Han, L.; González-Moreno, P.; Ma, H.; Ye, H.; Sobeih, T. A Deep Learning-Based Approach for Automated Yellow Rust Disease Detection from High-Resolution Hyperspectral UAV Images. *Remote Sens.* **2019**, *11*, 1554. [[CrossRef](#)]
101. Zhu, H.; Chu, B.; Zhang, C.; Liu, F.; Jiang, L.; He, Y. Hyperspectral Imaging for Presymptomatic Detection of Tobacco Disease with Successive Projections Algorithm and Machine-learning Classifiers. *Sci. Rep.* **2017**, *7*, 4125. [[CrossRef](#)]

102. Islam, M.; Anh Dinh.; Wahid, K.; Bhowmik, P. Detection of potato diseases using image segmentation and multiclass support vector machine. In Proceedings of the 2017 IEEE 30th Canadian Conference on Electrical and Computer Engineering (CCECE), Windsor, ON, Canada, 30 April–3 May 2017; pp. 1–4.
103. Goodfellow, I.; Pouget-Abadie, J.; Mirza, M.; Xu, B.; Warde-Farley, D.; Ozair, S.; Courville, A.; Bengio, Y. Generative Adversarial Nets. In *Advances in Neural Information Processing Systems*; Ghahramani, Z., Welling, M., Cortes, C., Lawrence, N., Weinberger, K.Q., Eds.; Curran Associates, Inc.: Red Hook, NY, USA, 2014; Volume 27, pp. 2672–2680.
104. Lu, J.; Ehsani, R.; Shi, Y.; de Castro, A.I.; Wang, S. Detection of multi-tomato leaf diseases (late blight, target and bacterial spots) in different stages by using a spectral-based sensor. *Sci. Rep.* **2018**, *8*, 2793. [[CrossRef](#)]
105. Del Fiore, A.; Reverberi, M.; Ricelli, A.; Pinzari, F.; Serranti, S.; Fabbri, A.; Bonifazi, G.; Fanelli, C. Early detection of toxigenic fungi on maize by hyperspectral imaging analysis. *Int. J. Food Microbiol.* **2010**, *144*, 64–71. [[CrossRef](#)] [[PubMed](#)]
106. Costa, J.M.; Grant, O.M.; Chaves, M.M. Thermography to explore plant–environment interactions. *J. Exp. Bot.* **2013**, *64*, 3937–3949. [[CrossRef](#)] [[PubMed](#)]
107. Zhu, W.; Chen, H.; Ciechanowska, I.; Spaner, D. Application of infrared thermal imaging for the rapid diagnosis of crop disease. *IFAC-PapersOnLine* **2018**, *51*, 424–430. [[CrossRef](#)]
108. Oerke, E.; Fröhling, P.; Steiner, U. Thermographic assessment of scab disease on apple leaves. *Precis. Agric.* **2011**, *12*, 699–715. [[CrossRef](#)]
109. Smigaj, M.; Gaulton, R.; Suárez, J.C.; Barr, S.L. Canopy temperature from an Unmanned Aerial Vehicle as an indicator of tree stress associated with red band needle blight severity. *For. Ecol. Manag.* **2019**, *433*, 699–708. [[CrossRef](#)]
110. Wen, D.M.; Chen, M.X.; Zhao, L.; Ji, T.; Li, M.; Yang, X.T. Use of thermal imaging and Fourier transform infrared spectroscopy for the pre-symptomatic detection of cucumber downy mildew. *Eur. J. Plant Pathol.* **2019**, *155*, 405–416. [[CrossRef](#)]
111. Jafari, M.; Minaei, S.; Safaie, N. Detection of pre-symptomatic rose powdery-mildew and gray-mold diseases based on thermal vision. *Infrared Phys. Technol.* **2017**, *85*, 170–183. [[CrossRef](#)]
112. Wang, M.; Ling, N.; Dong, X.; Zhu, Y.; Shen, Q.; Guo, S. Thermographic visualization of leaf response in cucumber plants infected with the soil-borne pathogen *Fusarium oxysporum* f. sp. *cucumerinum*. *Plant Physiol. Biochem.* **2012**, *61*, 153–161. [[CrossRef](#)] [[PubMed](#)]
113. Sankaran, S.; Mishra, A.; Maja, J.M.; Ehsani, R. Visible-near infrared spectroscopy for detection of Huanglongbing in citrus orchards. *Comput. Electron. Agric.* **2011**, *77*, 127–134. [[CrossRef](#)]
114. Liang, P.S.; Haff, R.P.; Hua, S.S.T.; Munyaneza, J.E.; Mustafa, T.; Sarreal, S.B.L. Nondestructive detection of zebra chip disease in potatoes using near-infrared spectroscopy. *Biosyst. Eng.* **2018**, *166*, 161–169. [[CrossRef](#)]
115. Gold, K.M.; Townsend, P.A.; Herrmann, I.; Gevens, A.J. Investigating potato late blight physiological differences across potato cultivars with spectroscopy and machine learning. *Plant Sci.* **2020**, *295*, 110316. [[CrossRef](#)]
116. Karadağ, K.; Tenekci, M.E.; Taşaltın, R.; Bilgili, A. Detection of pepper fusarium disease using machine learning algorithms based on spectral reflectance. *Sustain. Comput. Inform. Syst.* **2020**, *28*, 100299. [[CrossRef](#)]
117. Kafle, G.K.; Khot, L.R.; Jarolmasjed, S.; Yongsheng, S.; Lewis, K. Robustness of near infrared spectroscopy based spectral features for non-destructive bitter pit detection in honeycrisp apples. *Postharvest Biol. Technol.* **2016**, *120*, 188–192. [[CrossRef](#)]
118. Farber, C.; Kourouski, D. Detection and Identification of Plant Pathogens on Maize Kernels with a Hand-Held Raman Spectrometer. *Anal. Chem.* **2018**, *90*, 3009–3012. [[CrossRef](#)]
119. Yeturu, S.; Vargas Jentzsch, P.; Ciobotă, V.; Guerrero, R.; Garrido, P.; Ramos, L.A. Handheld Raman spectroscopy for the early detection of plant diseases: Abutilon mosaic virus infecting Abutilon sp. *Anal. Methods* **2016**, *8*, 3450–3457. [[CrossRef](#)]
120. Liu, Y.; Xiao, H.; Hao, Y.; Ye, L.; Jiang, X.; Wang, H.; Sun, X. Diagnosis of Citrus Greening using Raman Spectroscopy-Based Pattern Recognition. *J. Appl. Spectrosc.* **2020**, *87*, 150–158. [[CrossRef](#)]
121. Mandrile, L.; Rotunno, S.; Miozzi, L.; Vaira, A.M.; Giovannozzi, A.M.; Rossi, A.M.; Noris, E. Nondestructive Raman Spectroscopy as a Tool for Early Detection and Discrimination of the Infection of Tomato Plants by Two Economically Important Viruses. *Anal. Chem.* **2019**, *91*, 9025–9031. [[CrossRef](#)] [[PubMed](#)]
122. Murchie, E.; Lawson, T. Chlorophyll fluorescence analysis: A guide to good practice and understanding some new applications. *J. Exp. Bot.* **2013**, *64*, 3983–3998. [[CrossRef](#)]
123. Étienne Belin.; Rousseau, D.; Boureau, T.; Caffier, V. Thermography versus chlorophyll fluorescence imaging for detection and quantification of apple scab. *Comput. Electron. Agric.* **2013**, *90*, 159–163. [[CrossRef](#)]
124. Wang, L.; Poque, S.; Valkonen, J.P.T. Phenotyping viral infection in sweetpotato using a high-throughput chlorophyll fluorescence and thermal imaging platform. *Plant Methods* **2019**, *15*, 116. [[CrossRef](#)]
125. Bauriegel, E.; Herppich, W.B. Hyperspectral and Chlorophyll Fluorescence Imaging for Early Detection of Plant Diseases, with Special Reference to *Fusarium spec.* Infections on Wheat. *Agriculture* **2014**, *4*, 32–57. [[CrossRef](#)]
126. Pineda, M.; Pérez-Bueno, M.L.; Barón, M. Detection of Bacterial Infection in Melon Plants by Classification Methods Based on Imaging Data. *Front. Plant Sci.* **2018**, *9*, 164. [[CrossRef](#)]
127. Pan, X.; Welti, R.; Wang, X. Quantitative analysis of major plant hormones in crude plant extracts by high-performance liquid chromatography–mass spectrometry. *Nat. Protoc.* **2010**, *5*, 986–992. [[CrossRef](#)]
128. Müller, M.; Munné-Bosch, S. Rapid and sensitive hormonal profiling of complex plant samples by liquid chromatography coupled to electrospray ionization tandem mass spectrometry. *Plant Methods* **2011**, *7*, 37. [[CrossRef](#)]

129. Kojima, M.; Kamada-Nobusada, T.; Komatsu, H.; Takei, K.; Kuroha, T.; Mizutani, M.; Ashikari, M.; Ueguchi-Tanaka, M.; Matsuoka, M.; Suzuki, K.; et al. Highly Sensitive and High-Throughput Analysis of Plant Hormones Using MS-Probe Modification and Liquid Chromatography–Tandem Mass Spectrometry: An Application for Hormone Profiling in *Oryza sativa*. *Plant Cell Physiol.* **2009**, *50*, 1201–1214. [[CrossRef](#)]
130. Fang, Y.; Bullock, H.; Lee, S.A.; Sekar, N.; Eiteman, M.A.; Whitman, W.B.; Ramasamy, R.P. Detection of methyl salicylate using bi-enzyme electrochemical sensor consisting salicylate hydroxylase and tyrosinase. *Biosens. Bioelectron.* **2016**, *85*, 603–610. [[CrossRef](#)]
131. Martín, C.; Domínguez, E. A new enzyme electrode for quantification of salicylic acid in a FIA system. *J. Pharm. Biomed. Anal.* **1999**, *19*, 107–113. [[CrossRef](#)]
132. Chen, C.; Feng, S.; Zhou, M.; Ji, C.; Que, L.; Wang, W. Development of a structure-switching aptamer-based nanosensor for salicylic acid detection. *Biosens. Bioelectron.* **2019**, *140*, 111342. [[CrossRef](#)]
133. Yang, X.; Gao, Y.; Ji, Z.; Zhu, L.B.; Yang, C.; Zhao, Y.; Shu, Y.; Jin, D.; Xu, Q.; Zhao, W.W. Dual Functional Molecular Imprinted Polymer-Modified Organometal Lead Halide Perovskite: Synthesis and Application for Photoelectrochemical Sensing of Salicylic Acid. *Anal. Chem.* **2019**, *91*, 9356–9360. [[CrossRef](#)]
134. Rawlinson, S.; McLister, A.; Kanyong, P.; Davis, J. Rapid determination of salicylic acid at screen printed electrodes. *Microchem. J.* **2018**, *137*, 71–77. [[CrossRef](#)]
135. Park, J.; Eun, C. Electrochemical Behavior and Determination of Salicylic Acid at Carbon-fiber Electrodes. *Electrochim. Acta* **2016**, *194*, 346–356. [[CrossRef](#)]
136. Wang, H.R.; Bi, X.M.; Fang, Z.J.; Yang, H.; Gu, H.Y.; Sun, L.J.; Bao, N. Real time sensing of salicylic acid in infected tomato leaves using carbon tape electrodes modified with handed pencil trace. *Sens. Actuators B Chem.* **2019**, *286*, 104–110. [[CrossRef](#)]
137. Sun, L.J.; Feng, Q.M.; Yan, Y.F.; Pan, Z.Q.; Li, X.H.; Song, F.M.; Yang, H.; Xu, J.J.; Bao, N.; Gu, H.Y. Paper-based electroanalytical devices for in situ determination of salicylic acid in living tomato leaves. *Biosens. Bioelectron.* **2014**, *60*, 154–160. [[CrossRef](#)]
138. Xiong, X.J.; Rao, W.B.; Guo, X.F.; Wang, H.; Zhang, H.S. Ultrasensitive Determination of Jasmonic Acid in Plant Tissues Using High-Performance Liquid Chromatography with Fluorescence Detection. *J. Agric. Food Chem.* **2012**, *60*, 5107–5111. [[CrossRef](#)]
139. Gan, T.; Hu, C.; Chen, Z.; Hu, S. Fabrication and application of a novel plant hormone sensor for the determination of methyl jasmonate based on self-assembling of phosphotungstic acid–graphene oxide nanohybrid on graphite electrode. *Sens. Actuators B Chem.* **2010**, *151*, 8–14. [[CrossRef](#)]
140. Rustia, D.J.A.; Lin, C.E.; Chung, J.Y.; Zhuang, Y.J.; Hsu, J.C.; Lin, T.T. Application of an image and environmental sensor network for automated greenhouse insect pest monitoring. *J. Asia-Pac. Entomol.* **2020**, *23*, 17–28. [[CrossRef](#)]
141. Partel, V.; Nunes, L.; Stansly, P.; Ampatzidis, Y. Automated vision-based system for monitoring Asian citrus psyllid in orchards utilizing artificial intelligence. *Comput. Electron. Agric.* **2019**, *162*, 328–336. [[CrossRef](#)]
142. Selvaraj, M.G.; Vergara, A.; Ruiz, H.; Safari, N.; Elayabalan, S.; Ocimati, W.; Blomme, G. AI-powered banana diseases and pest detection. *Plant Methods* **2019**, *15*, 92. [[CrossRef](#)]
143. Liu, L.; Wang, R.; Xie, C.; Yang, P.; Wang, F.; Sudirman, S.; Liu, W. PestNet: An End-to-End Deep Learning Approach for Large-Scale Multi-Class Pest Detection and Classification. *IEEE Access* **2019**, *7*, 45301–45312. [[CrossRef](#)]
144. Deng, L.; Wang, Y.; Han, Z.; Yu, R. Research on insect pest image detection and recognition based on bio-inspired methods. *Biosyst. Eng.* **2018**, *169*, 139–148. [[CrossRef](#)]
145. Ebrahimi, M.; Khoshtaghaza, M.; Minaei, S.; Jamshidi, B. Vision-based pest detection based on SVM classification method. *Comput. Electron. Agric.* **2017**, *137*, 52–58. [[CrossRef](#)]
146. Ding, W.; Taylor, G. Automatic moth detection from trap images for pest management. *Comput. Electron. Agric.* **2016**, *123*, 17–28. [[CrossRef](#)]
147. Espinoza, K.; Valera, D.L.; Torres, J.A.; López, A.; Molina-Aiz, F.D. Combination of image processing and artificial neural networks as a novel approach for the identification of Bemisia tabaci and Frankliniella occidentalis on sticky traps in greenhouse agriculture. *Comput. Electron. Agric.* **2016**, *127*, 495–505. [[CrossRef](#)]
148. Liu, T.; Chen, W.; Wu, W.; Sun, C.; Guo, W.; Zhu, X. Detection of aphids in wheat fields using a computer vision technique. *Biosyst. Eng.* **2016**, *141*, 82–93. [[CrossRef](#)]
149. Redmon, J.; Farhadi, A. YOLOv3: An Incremental Improvement. *arXiv* **2018**, arXiv:1804.02767.
150. Yahia, E.M.; Neven, L.G.; Jones, R.W. Chapter 16—Postharvest Insects and Their Control. In *Postharvest Technology of Perishable Horticultural Commodities*; Yahia, E.M., 1st Ed.; Woodhead Publishing limited: Cambridge, UK, 2019; pp. 529–562.
151. Serre, T.; Wolf, L.; Bileschi, S.; Riesenhuber, M.; Poggio, T. Robust Object Recognition with Cortex-Like Mechanisms. *IEEE Trans. Pattern Anal. Mach. Intell.* **2007**, *29*, 411–426. [[CrossRef](#)] [[PubMed](#)]
152. Mankin, R.W.; Hagstrum, D.W.; Smith, M.T.; Roda, A.L.; Kairo, M.T.K. Perspective and Promise: A Century of Insect Acoustic Detection and Monitoring. *Am. Entomol.* **2011**, *57*, 30–44. [[CrossRef](#)]
153. Rach, M.M.; Gomis, H.M.; Granado, O.L.; Malumbres, M.P.; Campoy, A.M.; Martín, J.J.S. On the Design of a Bioacoustic Sensor for the Early Detection of the Red Palm Weevil. *Sensors* **2013**, *13*, 1706–1729. [[CrossRef](#)]
154. Escola, J.P.L.; Guido, R.C.; da Silva, I.N.; Cardoso, A.M.; Maccagnan, D.H.B.; Dezotti, A.K. Automated acoustic detection of a cicadid pest in coffee plantations. *Comput. Electron. Agric.* **2020**, *169*, 105215. [[CrossRef](#)]

155. Hetzroni, A.; Soroker, V.; Cohen, Y. Toward practical acoustic red palm weevil detection. *Comput. Electron. Agric.* **2016**, *124*, 100–106. [CrossRef]
156. Görres, C.M.; Chesmore, D. Active sound production of scarab beetle larvae opens up new possibilities for species-specific pest monitoring in soils. *Sci. Rep.* **2019**, *9*, 10115. [CrossRef]
157. Delory, B.M.; Delaplace, P.; Fauconnier, M.L.; du Jardin, P. Root-emitted volatile organic compounds: Can they mediate belowground plant-plant interactions? *Plant Soil* **2016**, *402*, 1–26. [CrossRef]
158. Bitas, V.; Kim, H.S.; Bennett, J.W.; Kang, S. Sniffing on Microbes: Diverse Roles of Microbial Volatile Organic Compounds in Plant Health. *Mol. Plant-Microbe Interact.* **2013**, *26*, 835–843. [CrossRef]
159. Brilli, F.; Loreto, F.; Baccelli, I. Exploiting Plant Volatile Organic Compounds (VOCs) in Agriculture to Improve Sustainable Defense Strategies and Productivity of Crops. *Front. Plant Sci.* **2019**, *10*, 264. [CrossRef]
160. Cui, S.; Inocente, E.A.A.; Acosta, N.; Keener, H.M.; Zhu, H.; Ling, P.P. Development of Fast E-nose System for Early-Stage Diagnosis of Aphid-Stressed Tomato Plants. *Sensors* **2019**, *19*, 3480. [CrossRef]
161. Farag, M.A.; Ryu, C.M.; Sumner, L.W.; Paré, P.W. GC-MS SPME profiling of rhizobacterial volatiles reveals prospective inducers of growth promotion and induced systemic resistance in plants. *Phytochemistry* **2006**, *67*, 2262–2268. [CrossRef]
162. Stoppacher, N.; Kluger, B.; Zeilinger, S.; Krska, R.; Schuhmacher, R. Identification and profiling of volatile metabolites of the biocontrol fungus *Trichoderma atroviride* by HS-SPME-GC-MS. *J. Microbiol. Methods* **2010**, *81*, 187–193. [CrossRef]
163. Brilli, F.; Ruuskanen, T.M.; Schnitzhofer, R.; Müller, M.; Breitenlechner, M.; Bittner, V.; Wohlfahrt, G.; Loreto, F.; Hansel, A. Detection of Plant Volatiles after Leaf Wounding and Darkening by Proton Transfer Reaction “Time-of-Flight” Mass Spectrometry (PTR-TOF). *PLoS ONE* **2011**, *6*, 1–12. [CrossRef]
164. Blake, R.S.; Monks, P.S.; Ellis, A.M. Proton-Transfer Reaction Mass Spectrometry. *Chem. Rev.* **2009**, *109*, 861–896. [CrossRef]
165. Portable Electronic Nose | AIRSENSE Analytics. Available online: <https://airsense.com/en/products/portable-electronic-nose> (accessed on 2 January 2021).
166. Neo Electronic Nose | Norlab. Available online: <https://www.norlab.com/library/brochure/11575> (accessed on 2 January 2021).
167. Sensigent. Available online: <http://www.sensigent.com/products/cyranose.html> (accessed on 2 January 2021).
168. Park, S.Y.; Kim, Y.; Kim, T.; Eom, T.H.; Kim, S.Y.; Jang, H.W. Chemoresistive materials for electronic nose: Progress, perspectives, and challenges. *InfoMat* **2019**, *1*, 289–316. [CrossRef]
169. Blasioli, S.; Biondi, E.; Braschi, I.; Mazzucchi, U.; Bazzi, C.; Gessa, C. Electronic nose as an innovative tool for the diagnosis of grapevine crown gall. *Anal. Chim. Acta* **2010**, *672*, 20–24. [CrossRef]
170. Cellini, A.; Biondi, E.; Blasioli, S.; Rocchi, L.; Farneti, B.; Braschi, I.; Savioli, S.; Rodriguez-Estrada, M.; Biasioli, F.; Spinelli, F. Early detection of bacterial diseases in apple plants by analysis of volatile organic compounds profiles and use of electronic nose. *Ann. Appl. Biol.* **2016**, *168*, 409–420. [CrossRef]
171. Li, Z.; Paul, R.; Ba Tis, T.; Saville, A.C.; Hansel, J.C.; Yu, T.; Ristaino, J.B.; Wei, Q. Non-invasive plant disease diagnostics enabled by smartphone-based fingerprinting of leaf volatiles. *Nat. Plants* **2019**, *5*, 856–866. [CrossRef]
172. Shang, L.; Liu, C.; Chen, B.; Hayashi, K. Development of molecular imprinted sol-gel based LSPR sensor for detection of volatile cis-jasmone in plant. *Sens. Actuators B Chem.* **2018**, *260*, 617–626. [CrossRef]
173. Wang, Z.; Chen, W.; Gu, S.; Wang, J.; Wang, Y. Discrimination of wood borers infested *Platyclusus orientalis* trunks using quartz crystal microbalance gas sensor array. *Sens. Actuators B Chem.* **2020**, *309*, 127767. [CrossRef]
174. Husin, N.A.; Khairunniza-Bejo, S.; Abdullah, A.F.; Kassim, M.S.M.; Ahmad, D.; Azmi, A.N.N. Application of Ground-Based LiDAR for Analysing Oil Palm Canopy Properties on the Occurrence of Basal Stem Rot (BSR) Disease. *Sci. Rep.* **2020**, *10*, 6464. [CrossRef] [PubMed]
175. Giannakis, I.; Tosti, F.; Lantini, L.; Alani, A.M. Diagnosing Emerging Infectious Diseases of Trees Using Ground Penetrating Radar. *IEEE Trans. Geosci. Remote Sens.* **2020**, *58*, 1146–1155. [CrossRef]
176. Junttila, S.; Holopainen, M.; Vastaranta, M.; Lyytikäinen-Saarenmaa, P.; Kaartinen, H.; Hyypä, J.; Hyypä, H. The potential of dual-wavelength terrestrial lidar in early detection of *Ips typographus* (L.) infestation—Leaf water content as a proxy. *Remote Sens. Environ.* **2019**, *231*, 111264. [CrossRef]
177. Zhang, X.; Derival, M.; Albrecht, U.; Ampatzidis, Y. Evaluation of a Ground Penetrating Radar to Map the Root Architecture of HLB-Infected Citrus Trees. *Agronomy* **2019**, *9*, 354. [CrossRef]
178. Pham, H.; Lim, Y.; Gardi, A.; Sabatini, R. A Novel Bistatic LIDAR System for Early-Detection of Plant Diseases from Unmanned Aircraft. In Proceedings of the 31th Congress of the International Council of the Aeronautical Sciences (ICAS 2018)At, Belo Horizonte, Brazil, September 18, 2018.
179. Lin, Y. LiDAR: An important tool for next-generation phenotyping technology of high potential for plant phenomics? *Comput. Electron. Agric.* **2015**, *119*, 61–73. [CrossRef]
180. Omasa, K.; Hosoi, F.; Konishi, A. 3D lidar imaging for detecting and understanding plant responses and canopy structure. *J. Exp. Bot.* **2006**, *58*, 881–898. [CrossRef]
181. Delgado, A.; Hays, D.B.; Bruton, R.K.; Ceballos, H.; Novo, A.; Boi, E.; Selvaraj, M.G. Ground penetrating radar: A case study for estimating root bulking rate in cassava (*Manihot esculenta* Crantz). *Plant Methods* **2017**, *13*, 65. [CrossRef]

-
182. Malmqvist, E.; Jansson, S.; Zhu, S.; Li, W.; Svanberg, K.; Svanberg, S.; Rydell, J.; Song, Z.; Bood, J.; Brydegaard, M.; Åkesson, S. The bat–bird–bug battle: Daily flight activity of insects and their predators over a rice field revealed by high-resolution Scheimpflug Lidar. *R. Soc. Open Sci.* **2018**, *5*, 172303.
 183. Agriculture IoT Market - Global Opportunity Analysis and Industry Forecast (2019–2027). Available online: <https://www.meticulousresearch.com/product/agriculture-iot-market-5080/> (accessed on 13 January 2021).